MicroRNA-214 controls skin and hair follicle development by modulating the activity of the Wnt pathway

Mohammed I. Ahmed,[1]* Majid Alam,[1]* Vladimir U. Emelianov,[2] Krzysztof Poterlowicz,[1] Ankit Patel,[1] Andrey A. Sharov,[2] Andrei N. Mardaryev,[1] and Natalia V. Botchkareva[1]

[1]Centre for Skin Sciences, School of Life Sciences, University of Bradford, Bradford BD7 1DP, England, UK
[2]Department of Dermatology, Boston University, Boston, MA 02118

Skin development is governed by complex programs of gene activation and silencing, including microRNA-dependent modulation of gene expression. Here, we show that miR-214 regulates skin morphogenesis and hair follicle (HF) cycling by targeting β-catenin, a key component of the Wnt signaling pathway. miR-214 exhibits differential expression patterns in the skin epithelium, and its inducible overexpression in keratinocytes inhibited proliferation, which resulted in formation of fewer HFs with decreased hair bulb size and thinner hair production. The inhibitory effects of miR-214 on HF development and cycling were associated with altered activities of multiple signaling pathways, including decreased expression of key Wnt signaling mediators β-catenin and Lef-1, and were rescued by treatment with pharmacological Wnt activators. Finally, we identify β-catenin as one of the conserved miR-214 targets in keratinocytes. These data provide an important foundation for further analyses of miR-214 as a key regulator of Wnt pathway activity and stem cell functions during normal tissue homeostasis, regeneration, and aging.

Introduction

Skin development is a complex dynamic process that results in formation of the epidermis, a stratified self-renewed epithelium, and several skin appendages including hair follicles (HFs), nails, and glands (Blanpain and Fuchs, 2009). HF morphogenesis is driven by bidirectional ectodermal–mesenchymal interactions between epidermal keratinocytes and a specialized population of dermal fibroblasts, and results in formation of the hair bulb, in which epithelial progenitor cells proliferate and differentiate into six distinct cell lineages to form the hair shaft and its supporting layers of the inner root sheath (Millar, 2002; Schmidt-Ullrich and Paus, 2005; Blanpain and Fuchs, 2009). HF morphogenesis is governed by a well-balanced interplay between cell proliferation, differentiation, and apoptosis, which are controlled at several levels including signaling/transcription factor-mediated and epigenetic regulatory mechanisms (Millar, 2002; Schmidt-Ullrich and Paus, 2005; Blanpain and Fuchs, 2009; Botchkarev et al., 2012; Frye and Benitah, 2012).

During postnatal life, HFs undergo cyclic regeneration with periods of active growth (anagen), regression (catagen), and relative resting (telogen; Stenn and Paus, 2001; Schneider et al., 2009). Initiation of a new growth phase in resting HFs occurs as a result of signaling exchange between epithelial stem cells residing in the bulge/secondary hair germ and dermal papilla fibroblasts, and is driven by the growth stimulatory molecules (Wnt ligands, BMP inhibitors, Shh, TGF-β2, FGF7, FGF10), the effects of which predominate over the growth inhibitory signals generated by the BMP ligands or FGF18 (Hsu and Fuchs, 2012).

In addition to signaling/transcription factor–mediated and epigenetic regulatory mechanisms, programs of gene activation and silencing governing HF development and cycling are controlled by microRNAs (miRNAs; Yi and Fuchs, 2011; Botchkareva,

*Mohammed I. Ahmed and Majid Alam contributed equally to this paper.

Correspondence to Natalia V. Botchkareva: n.botchkareva@bradford.ac.uk

Abbreviations used in this paper: BIO, 6-bromoindirubin-3′-oxime; Dox, doxycycline; DTG, double transgenic K14-rtTA/miR-214-TRE; E, embryonic day; HF, hair follicle; P, postnatal day; PMEK, primary mouse epidermal keratinocyte; WT, wild type.

The Rockefeller University Press $30.00
J. Cell Biol. Vol. 207 No. 4 549–567
www.jcb.org/cgi/doi/10.1083/jcb.201404001

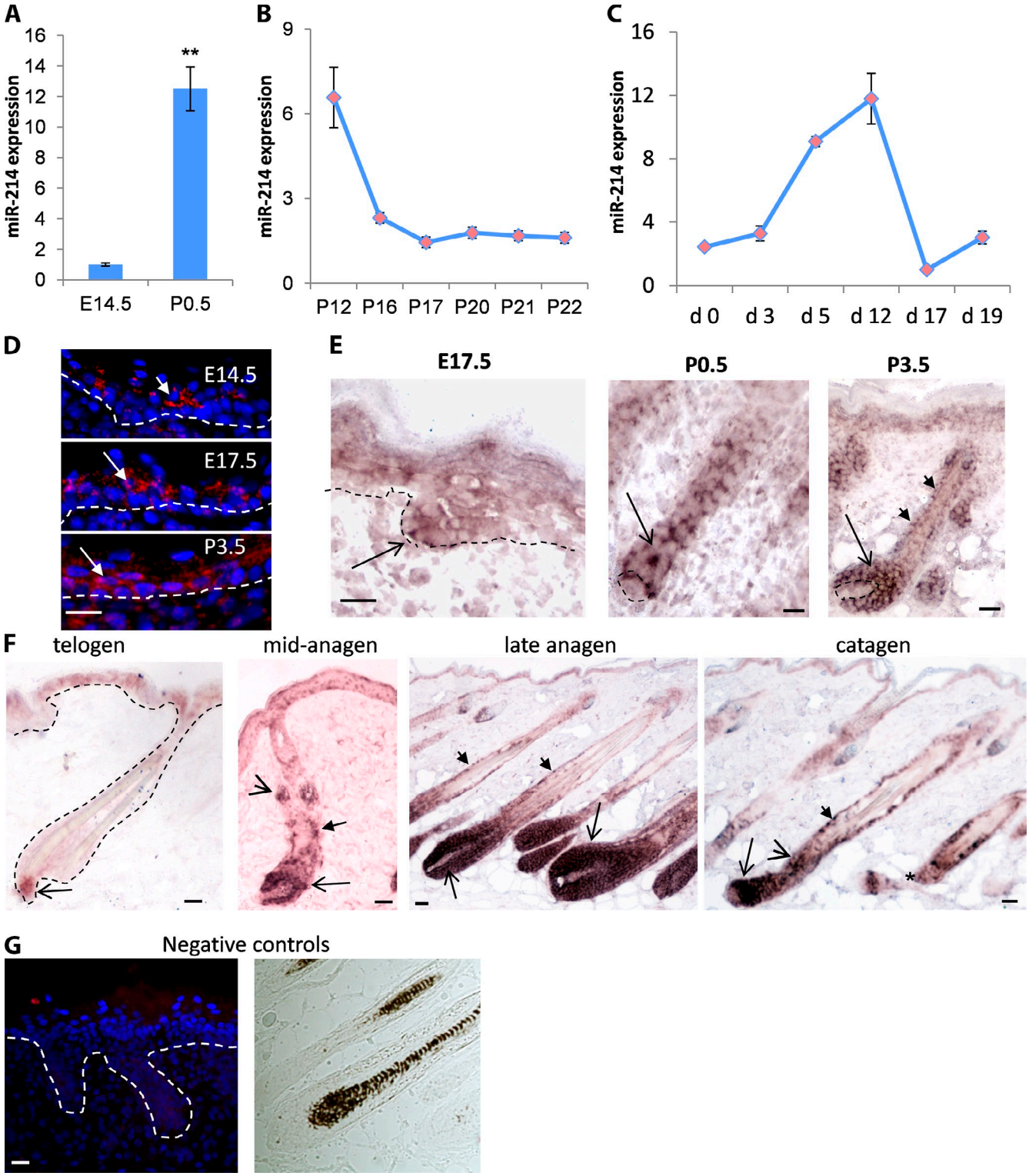

Figure 1. **Spatiotemporal expression of miR-214 during HF morphogenesis and cycling.** (A–C) TaqMan real-time RT-PCR analysis of miR-214 expression. (A) miR-214 levels in in the skin of newborn mice at P0.5 compared with embryonic skin at E14.5. *n* = 3 mice for each time point. Data are presented as mean ± SD (error bars); **, P < 0.01; Student's *t* test. (B) miR-214 levels in skin during the postnatal hair cycle: anagen-like stage (P12), catagen (P16–P17), and telogen (P20–P22). *n* = 2 mice for each time point. Data are presented as mean ± SEM (error bars). (C) miR-214 in depilation-induced hair cycle: telogen (day 0), anagen (days 3–12), and catagen (days 17–19). *n* = 2 mice for each time point. Data are presented as mean ± SEM (error bars). (D–G) miR-214 in situ hybridization. (D) miR-214 in the developing epidermis using Tyramide Signal Amplification for fluorescent detection. miR-214 expression was detected in the suprabasal epidermal layers at E14.5 (arrow); more prominent miR-214 signal is visible throughout the epidermis at E17.5 and P3.5 (arrows). The broken lines demarcate the epidermal–dermal border. (E) HF morphogenesis. miR-214 appears in the developing hair placodes at E17.5 (arrow). At P0.5, miR-214 is expressed throughout the epithelium of stage 3–6 HFs (arrow). In fully developed HFs (stage 8, P3.5), miR-214 expression increased in the developing hair matrix (arrow) and individual cells of the outer root sheath (arrowheads). (F) Hair cycle. miR-214 is expressed in telogen secondary germ (arrow), and appears in the hair matrix (arrow), outer root sheath (small arrow), and in the bulge area (arrowheads)

2012; Ning and Andl, 2013). miRNAs largely contribute to the regulation of gene expression by fine tuning and buffering the activity of signaling pathways. miRNAs interact with their target complimentary messenger RNAs by base-pairing between 5′ end sequences of miRNAs and mRNAs sequences located in the 3′ untranslated region (3′ UTR), which leads to either mRNA destabilization, the inhibition of translation initiation, or both (Lee et al., 1993; Ambros, 2001). In turn, the expression of miRNA can be controlled by cell type–specific transcription factors, and a major constituent of the miRNA processing machinery, Dicer, serves as a target gene of p63 and microphthalmia-associated transcription factor (MITF) in epithelial cells and melanocytes, respectively (Levy et al., 2010; Su et al., 2010). In addition, miRNAs can alter activities of the signaling pathways not only by targeting their genes, but also by acting as their downstream components (Ahmed et al., 2011). Therefore, miRNAs and their targets represent remarkably diverse regulatory networks, playing a key role in the execution of gene expression programs in stem cells and their progenies (Ambros, 2001; Inui et al., 2010).

Recent data demonstrated critical roles of miRNAs in controlling the activity of cutaneous stem cells and their lineage-committed progenies that drive skin development and regeneration (Yi and Fuchs, 2011; Botchkareva, 2012; Ning and Andl, 2013). Early studies by Andl et al. (2006) and Yi et al. (2006) have identified ∼70 miRNAs expressed in mouse embryonic skin. We have recently shown that expression levels of >200 miRNAs are changed during HF cyclic regeneration in mouse skin (Mardaryev et al., 2010). These findings suggest that miRNAs play a powerful role in the control of gene expression programs during skin development and hair cycle–associated tissue remodeling. Indeed, constitutive epidermal-specific deletion of the miRNA processors *Dicer* or *Dgcr8* results in the severe abnormalities in HF development characterized by the inability of the HFs to invaginate into the dermis (Andl et al., 2006; Yi et al., 2006). Inducible epidermal deletion of *Dicer* or *Drosha* in postnatal mouse skin has also demonstrated the crucial importance of miRNAs in the maintenance of the normal HF growth cycle (Teta et al., 2012).

Individual miRNAs are involved in controlling the expression of several key regulators of stem cell activity in the skin and HFs: miR-203 controls the proliferative potential of epithelial precursor cells by direct inhibition of p63 expression (Lena et al., 2008; Yi et al., 2008), and miR-125b serves as a rheostat that controls stem cell proliferation, fate commitment, and differentiation (Zhang et al., 2011), while miR-205 is indispensable for stem cell survival (Wang et al., 2013a). miR-31 is highly expressed in the HF during the anagen phase and controls hair cycle–associated tissue remodeling by regulating the expression of several important components of the Wnt, BMP, and FGF signaling pathways (Mardaryev et al., 2010).

Although substantial progress has been made in discovering the important players controlling skin and HF development and cycling, understanding the molecular mechanisms involved in the establishment of signaling/transcription networks in the keratinocytes still requires additional efforts. In this study, we aimed to explore a role of miR-214 in HF development and cycling. Yi et al. (2006) showed that miR-214 is one of the most abundant miRNAs expressed in the HFs of embryonic day 17.5 (E17.5) embryonic skin. Mouse miR-214 is encoded by a primary transcript Dynamin3-opposite strand (Dnm3os; Liu et al., 2010), deletion of which leads to skeletal abnormalities and a lethal phenotype (Watanabe et al., 2008). The expression of the miR-214 gene is developmentally regulated by Twist-1, a key transcriptional factor controlling epithelial–mesenchymal transitions (Lee et al., 2009), which is crucial for normal development and tissue repair. It has also been demonstrated that miR-214 plays an important role in controlling the development of the nervous system, teeth, the pancreas, and bone formation (Joglekar et al., 2007; Chen et al., 2010; Sehic et al., 2011; Wang et al., 2013b). However, its role in the control of skin and HF development and homeostasis is unknown.

In this study, we demonstrate that miR-214 show distinct expression patterns in the developing epidermis and HF. Keratinocyte-specific miR-214 overexpression causes a marked decrease in the number of HFs in developing skin, and a delay in anagen progression during postnatal development, which is associated with inhibition of cell proliferation in the epidermis and HFs. These effects are accompanied by dramatic changes in the gene expression and activity of different signaling pathways including Wnt, Shh, Eda, and Bmp, and are rescued by the administration of Wnt pathway activators. Furthermore, we identified β-catenin as a direct miR-214 target, which suggests that miR-214 is an important regulator of Wnt signaling pathway activity in developing and postnatal skin.

Results

miR-214 exhibits distinct expression patterns in the epidermis and HFs in developing and postnatal skin

To understand the role of miR-214 in the control of skin morphogenesis and HF cycling, miR-214 expression was examined in mouse back skin at different developmental stages, as well as during the first postnatal and depilation-induced hair cycles. Low levels of miR-214 expression were detected in embryonic skin at E14.5 during onset of the HF development, while its expression was dramatically elevated in the total skin of newborn mice containing HFs at different stages of development (Fig. 1 A). High miR-214 expression levels were maintained in the skin until P12, while its expression was decreased significantly during HF transition to the first regressing phase (catagen, P16-17)

in mid-anagen HF. In late anagen, prominent expression of miR-214 in the hair matrix (arrows) and in the outer root sheath (arrowheads) is seen. In catagen, miR-214 is expressed in the regressing hair matrix (arrow), outer root sheath (small arrow), and in the epithelial strand of the mid-catagen HF (arrowheads), whereas it disappears from the epithelial strand in the advanced catagen HFs (asterisk). (G) The scramble negative control using Tyramide (left) and chromogenic (right) detections. The broken line demarcates the epidermal–dermal border. Bars: (D) 25 µm; (E, left two panels) 25 µm; (E, right) 50 µm; (F) 50 µm; (G) 25 µm.

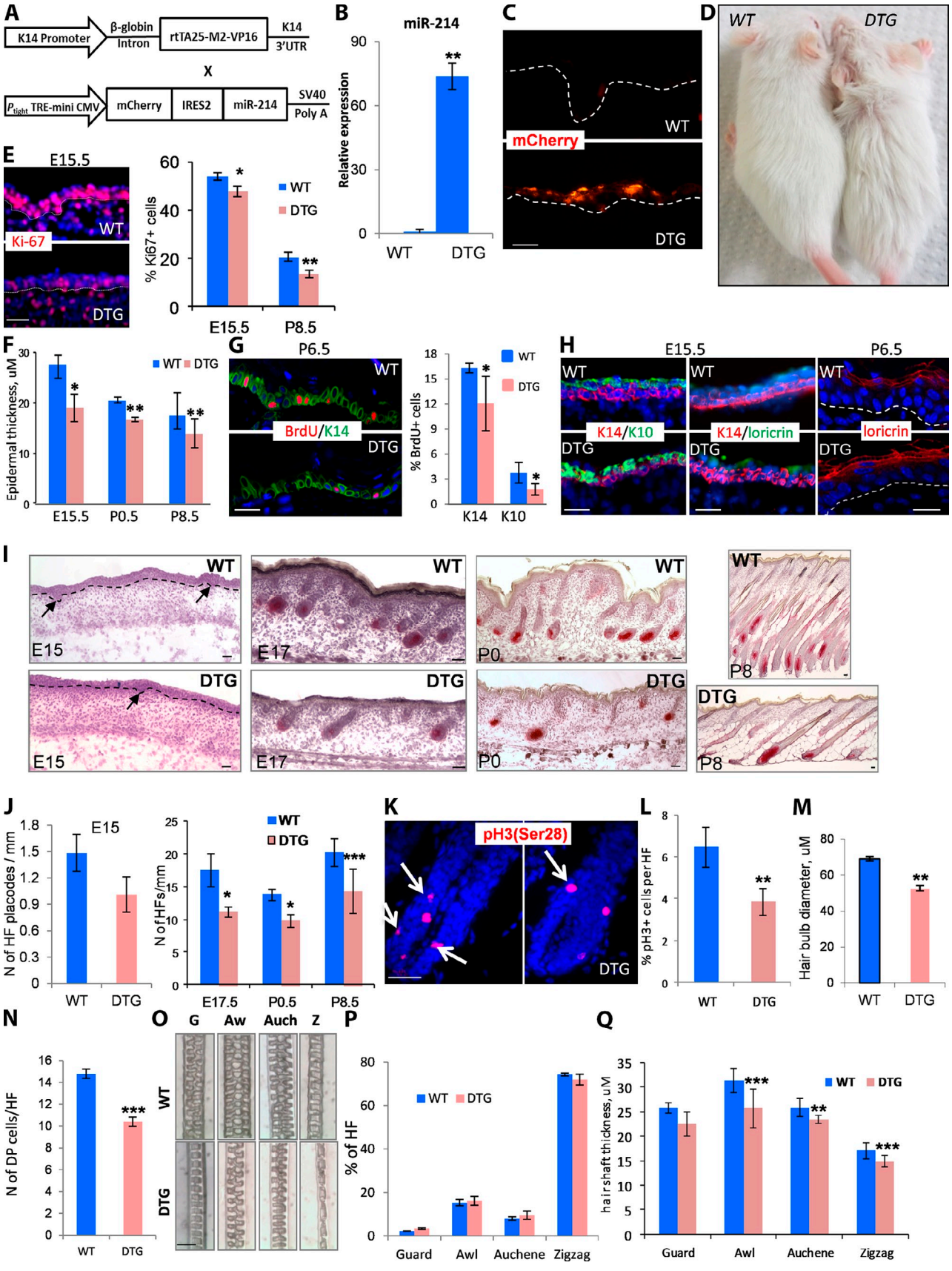

Figure 2. **Inhibitory effects of miR-214 on skin and HF morphogenesis.** (A) Schematic representation of the constructs for generation of K14-rtTA/miR-214-TRE (DTG) mice. (B) Real-time RT-PCR. There were increased levels of miR-214 in the skin of neonatal DTG mice at P0. *n* = 3 mice/genotype. (C) mCherry fluorescence in the epithelium of DTG mice at E15.5 after activation by Dox after E10.5. The broken lines demarcate the epidermal–dermal border.

and remained low during subsequent resting phase (telogen; P20-22; Fig. 1 B). Similar fluctuations in the miR-214 levels were observed in adult skin during depilation-induced hair cycle: miR-214 expression progressively increased during HF transition from telogen to anagen and was maximal during the late anagen stage of the hair cycle (day 12 after depilation) followed by rapid decrease during catagen (Fig. 1 C).

In situ hybridization analysis showed that in E14.5 and E17.5 skin, miR-214 expression was seen in the suprabasal epidermal layers, whereas in postnatal day 3.5 (P3.5) skin, relatively weak miR-214 expression was also seen in the basal epidermal layer (Fig. 1 D). miR-214 was abundantly expressed throughout the epithelium in the HF placodes and during more advanced stages of HF morphogenesis (E17.5–P0.5; Fig. 1 E; see Fig. 7 E). In fully developed HFs, miR-214 expression substantially increased in the developing hair matrix and individual cells of the outer root sheath (P3.5; Fig. 1 E).

During HF cycling, miR-214 expression was restricted to the secondary germ of the telogen HFs, while in early anagen HFs, miR-214 expression appeared in the growing hair matrix, the outer root sheath, and in the bulge area (Fig. 1 F). In fully developed anagen HFs, miR-214 was prominently expressed in the hair matrix, as well as in the distinct cells of the outer root sheath (Fig. 1 F; see Fig. 7 E). During catagen, miR-214 expression was seen in the regressing hair matrix, outer root sheath, and in the epithelial strand of the mid-catagen HF, whereas its expression disappeared from the epithelial strand at the advanced catagen stages (Fig. 1 F). These data suggest that miR-214 exhibits discrete expression patterns in selected epithelial compartments of the skin: it is predominantly localized in the suprabasal epidermal layers and in the epithelium of the developing HFs, as well as in the secondary germ of telogen HFs and hair matrix of anagen HFs.

Krt14-driven miR-214 overexpression results in alterations of epidermal and HF development

To amplify the miR-214 effects on the epithelial progenitor cell population located in the basal epidermal layer and HF outer root sheath, where miR-214 was relatively underexpressed compared with more the differentiated keratinocytes of the suprabasal epidermal layer and HF matrix keratinocytes (Fig. 1, D–F), mice overexpressing miR-214 under the control of doxycycline (Dox)-inducible Krt14-promoter (K14-rtTA/miR-214-TRE double transgenic [DTG]) were generated (Fig. 2 A). Induction of transgene by Dox starting from E10.5, which corresponds to the onset of Krt14 expression in the developing epidermis (Byrne et al., 1994), caused a dramatic increase in the level of miR-214 in the skin of DTG mice. This was confirmed by RT-qPCR (Fig. 2 B). Transgene expression was also confirmed by mCherry fluorescence in the basal epidermal layer of E15.5 skin (Fig. 2 C).

DTG mice were viable, fertile, and showed appearance of a "rough" fur coat postnatally (Fig. 2 D).

Between E15.5 and P8.5, DTG mice showed significantly decreased epidermal proliferation and thinner epidermis compared with wild type (WT) controls (Fig. 2, E and F). When P6 DTG and WT mice were pulsed with BrdU for 12 h followed by the costaining of BrdU and either K14 or K10, the majority of BrdU-positive cells were seen in the basal K14+ cells in both DTG and WT mice. However, it was a significant reduction in the number of BrdU+ cells in both basal and suprabasal epidermal layers of DTG mice compared with WT control (Fig. 2 G).

The expression of Keratin 14, Keratin 10, and Loricrin in basal or suprabasal epidermal layers, respectively, was quite similar in E15.5 DTG mice compared with WT mice (Fig. 2 H). However, Dox-treated epidermis of newborn DTG mice exhibited the increase of *Lor* transcript compared with the control (Fig. S1 A). Also, increased Loricrin protein expression was seen in the upper layers of the epidermis of the P6.5 DTG mice versus age-matched WT mice (Fig. 2 H). Therefore, decreased epidermal thickness in miR-214 DTG mice could be developed because of the reduced keratinocyte proliferation and accelerated terminal differentiation in the epidermis.

Interestingly, miR-214 overexpression caused a lack of ∼30% of HFs in the back skin (Fig. 2, I and J). The number of induced HFs was significantly decreased in DTG mice at E15.5, E17.5, P0.5, and P8.5 compared with WT controls (Fig. 2, I and J), which suggests that miR-214 overexpression alters the induction process in both primary and secondary HFs. The rate of HF development was not significantly different between DTG and WT mice; all HFs in DTG and WT mice reached the first anagen phase at P8.5 (Fig. 2 I). However, all transgenic HFs at P8.5 showed significantly reduced length, which was

(D) DTG and WT littermates were given Dox after E10.5 and photographed at P15. (E) Immunofluorescence of Ki-67 (red) in the epidermis of E15 skin with nuclear staining (DAPI, blue). There was a significant decrease of Ki-67+ cells at E15 and P8.5 in DTG epidermis. $n = 3$ mice/genotype for each time point. (F) Decrease in the epidermal thickness in DTG mice at E15, P0.5, and P8.5. $n = 3$ mice/genotype for each time point. (G) Immunofluorescence of BrdU (red) and K14 (green) in the epidermis of P6 skin with nuclear staining (DAPI, blue). There was a significant reduction in BrdU+ cells in both basal and suprabasal epidermal layers of DTG versus WT mice. $n = 3$ mice/genotype for each time point. (H) Immunofluorescence of K14 (red), K10 (green), and Loricrin (green) in the E15.5 epidermis and Loricrin (red) in the P6.5 epidermis with nuclear staining (DAPI, blue). There were no differences in the expression of K14, K10, and Loricirin between DTG and WT in E15 skin. There was increased Loricrin expression in DTG epidermis at P6.5. (I) Representative microphotographs of back skin histology of DTG and WT mice at different embryonic and postnatal days of skin and HF development. Arrows indicate HF placodes, and the broken lines demarcate the epidermal–dermal border. (J) Quantification of the total HF number per millimeter of skin in DTG versus WT littermate at E15, E17, P0.5, and P8.5. $n = 3$ mice/genotype for each time point. (K) Immunodetection of pH3(Ser28) (red) with nuclear staining (DAPI, blue) in the hair bulbs of DTG and WT mice at P8.5. (L) Quantification of a ratio of pH3(Ser28)+ to total cell number in the hair matrix at P8.5. $n = 3$ mice/genotype. (M) Significant reduction in hair bulb diameter in the DTG HFs at P8. $n = 3$ mice/genotype. (N) Quantification of the number of dermal papilla cells at P8.5. $n = 3$ mice/genotype. (O) Representative images of the different hair shaft types (guard, awl, auchene, and zigzag) plucked from telogen HFs of DTG and WT mice at P20. G, guard; Aw, awl; Ach, auchene; Z, zigzag. (P) Quantification of the number of different hair shaft types in DTG and WT mice. No difference between DTG and WT mice was detected. $n = 4$ mice/genotype. (Q) Significant decrease in the hair shaft thickness of the awl, auchene, and zigzag hairs in DTG versus WT mice. $n = 4$ mice/genotype. Data are presented as mean ± SD (error bars); *, $P < 0.05$; **, $P < 0.01$; ***, $P < 0.001$; Student's *t* test. Bars: (C, E, I, K, and O) 50 µm; (G and H) 25 µm.

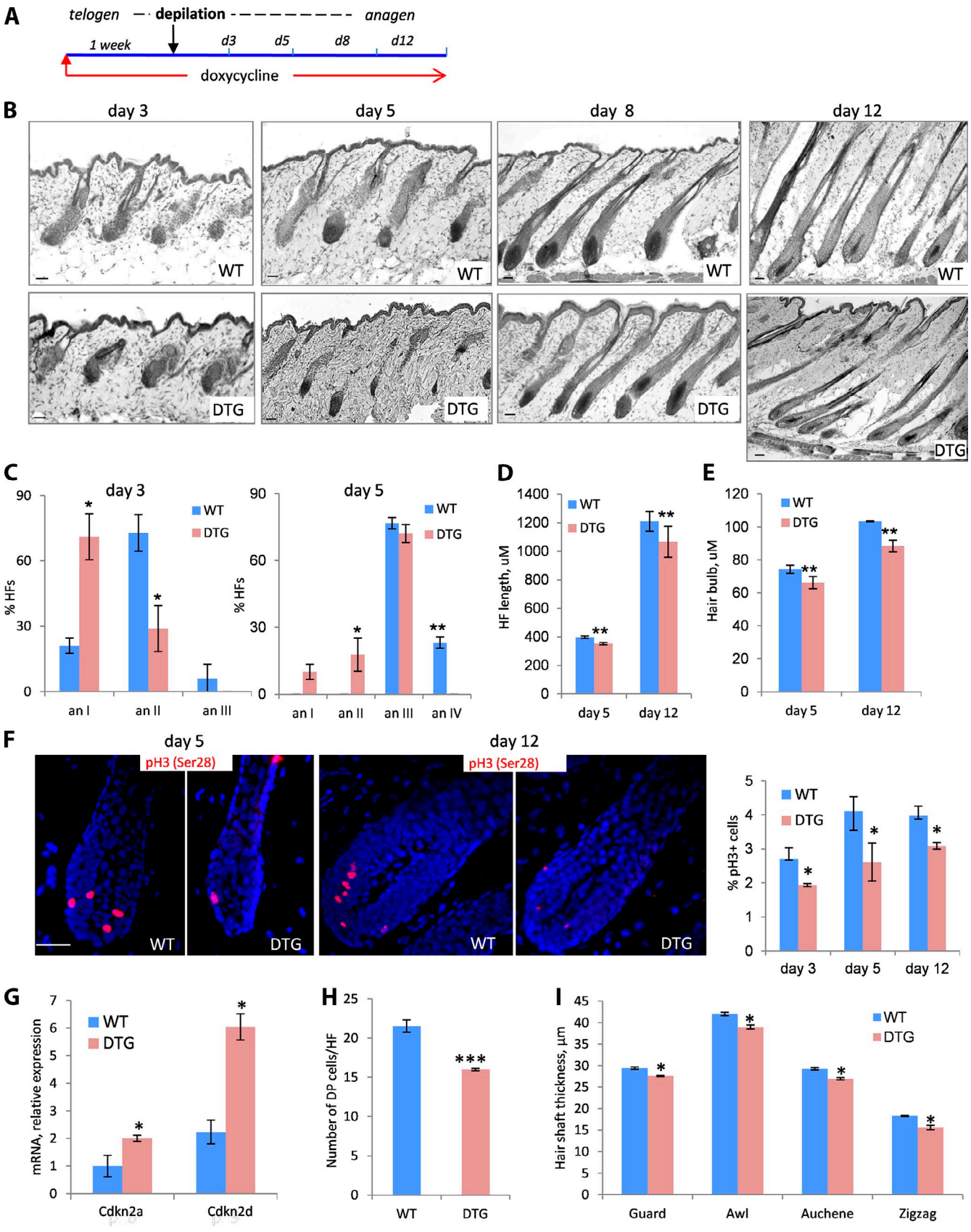

Figure 3. **Gain of miR-214 function inhibits hair cycle progression.** (A) Schematic illustration of the experimental design. (B) Representative microphotographs of back skin histology of DTG and WT mice at different days of a depilation-induced hair cycle. Bars, 50 µm. (C) Quantitative histomorphometry of HFs at different anagen substages at days 3 and 5 after depilation in DTG and WT mice. *n* = 5 mice/genotype for each time point. (D) Quantification of HF length at days 5 and 12 after depilation. *n* = 5 mice/genotype for each time point. (E) Quantification of hair bulb diameter in the HFs at day 5 and 12 after

accompanied by markedly reduced total skin thickness (Fig. S1, B and C). The hair bulb size and cell proliferation in the HF matrix were significantly reduced in all HFs of DTG mice versus the WT HFs (Fig. 2, I and K–M), whereas no apoptotic cells were detected in the HFs or interfollicular epidermis in DTG or WT mice (not depicted). In addition, a significant decrease in the number of dermal papilla cells was observed in transgenic HFs versus the corresponding controls (Fig. 2 N).

Despite the fact that the proportions of the guard, awl, auchen, and zigzag hair in DTG mice were similar to WT mice (Fig. 2, O and P), morphometric analyses of their hair shafts (P20; telogen HFs) revealed a significant decrease of their thickness but not the length in DTG versus WT mice (Fig. 2 Q and Fig. S1 D). Therefore, the changes in visual coat appearance in DTG mice were most likely caused by the reduced number of the HFs, as well as by the decreased thickness of the hair shafts induced by miR-214 overexpression.

Gain of miR-214 activity in postnatal skin alters HF cycling and HF size

To explore the effects of miR-214 on HF cycling, DTG mice were treated with Dox during telogen phase followed by the induction of the hair cycle by depilation (Fig. 3 A). Although telogen–anagen transition was initiated in DTG mice, they exhibited a significant delay in early anagen development compared with WT control (days 3 and 5 after depilation; Fig. 3, B and C). Anagen VI HFs were significantly shorter in DTG mice compared with WT mice (Fig. 3 D). On days 5–12 after depilation, the size of hair bulbs in DTG HFs was significantly reduced compared with WT controls (Fig. 3 E). These changes were associated with significantly decreased cell proliferation in the hair matrix and increased transcript levels of the cyclin-dependent kinase inhibitors *Cdkn2a (p16)* and *Cdkn2d (p19)* in DTG skin compared with WT mice (Fig. 3, F and G). Analysis of apoptosis by the detection of active caspase-3 did not reveal any differences between HFs in DTG and WT mice (Fig. S1 E). The number of dermal papilla cells in transgenic anagen VI HFs was significantly reduced (Fig. 3 H). Similar to HF morphogenesis, anagen DTG HFs produced significantly thinner hair shafts compared with WT controls (Fig. 3 I). These data suggest that miR-214 exerts its effects on HF development and cycling by modulation of keratinocyte proliferation and differentiation, as well as by regulating epithelial–mesenchymal interactions in the HF including the control of dermal papilla cell number.

miR-214 overexpression induces complex changes in gene expression programs in keratinocytes

To explore molecular mechanisms underlying the phenotype in miR-214 transgenic mice and identify potential targets of miR-214 in the keratinocytes, global mRNA expression profiling was performed in the back skin epithelium of neonatal DTG mice (P2.5), which received Dox for 48 h before skin collection (Fig. 4 A). The raw microarray expression profiles were background corrected and normalized with Bioconductor package limma (Smyth, 2005), and genes with more than twofold expression change in the epithelium of DTG mice compared with WT controls were identified as differentially expressed (Fig. 4 B). The in-house functional ontology database was used to categorize differentially expressed genes into the set of 12 distinct functional categories (Lewis et al., 2014). Bioinformatic analysis revealed twofold and higher changes in expression of 1,026 genes in skin epithelium of DTG versus WT mice (Fig. 4 B and Tables S1 and S2). Differentially expressed genes that belong to the "cell cycle" and "signaling" categories were further validated by RT-qPCR.

Using RT-qPCR, we confirmed that the transcript levels of *Ccnb1*, *Ccnd1*, *Ccnd2*, and *Cdk1* (cyclin B1, cyclin D1, cyclin D2, and cyclin-dependent kinase 1) were significantly lower in DTG mice compared with the WT littermates (Fig. 4 C). These data suggest that miR-214 indeed exerts inhibitory effects on cell proliferation, which were consistent with the epidermal and HF phenotypes seen in DTG mice (Figs. 2 and 3).

Interestingly, microarray analysis revealed changes in the expression of the genes encoding the components of several signaling pathways that are crucial for HF development and cycling, such as Wnt, Shh, Edar, and Bmp (Botchkarev and Paus, 2003; Schmidt-Ullrich et al., 2006; Blanpain and Fuchs, 2009). RT-qPCR confirmed significant down-regulation of the *Ctnnb1* and *Lef-1* expressions in the skin of DTG mice, which suggests inhibition of Wnt signaling activity induced by miR-214. Also, expressions of several genes that belong to Hedgehog signaling, such as *Shh* and its receptors *Smo* and *Ptch2*, were dramatically decreased in the epithelium of DTG versus WT mice. In addition, overexpression of miR-214 led to a significant decrease in the expression of *Edar* and the BMP inhibitor *Sostdc1* (Fig. 4 C). These data provide evidence that the effects of miR-214 on HF development and cycling are mediated, at least in part, by genes that control keratinocyte proliferation and mediate activity of key signaling pathways (Wnt, Hedgehog, Bmp, and Edar) known to be crucial for skin development and hair growth.

miR-214 overexpression in epithelial progenitor cells alters expression of key regulators of HF development and cycling

To further investigate the effects of gain of miR-214 functions on the activity of selected signaling pathways in skin, we analyzed the pattern of the expression of their different components in embryonic and postnatal skin of DTG and age-matched WT mice. Quantitative immunofluorescence analysis revealed the

depilation. *n* = 5 mice/genotype for each time point. (F) Immunodetection of pH3(Ser28) (red) in the hair bulbs of DTG and WT mice with nuclear staining (DAPI, blue). A significant reduction in the number of pH3(Ser28)+ cells in the HF of DTG mice at days 3, 5, and 12 after depilation was seen. *n* = 5 mice/genotype for each time point. Bar, 50 µm. (G) Real-time RT-PCR analysis of *Cdkn2a* and *Cdkn2d* expression at day 12 after depilation. *n* = 3 mice/genotype. (H) Quantification of the number of dermal papilla cells in anagen HFs at day 12 after depilation. *n* = 5 mice/genotype for each time point. (I) Quantification of the hair shaft thickness of the awl, auchene, and zigzag hairs in DTG versus WT mice plucked after the hair cycle completion at day 20 after depilation. *n* = 5 mice/genotype. Data are presented as mean ± SD (error bars); *, P < 0.05; **, P < 0.01; ***, P < 0.001; Student's *t* test.

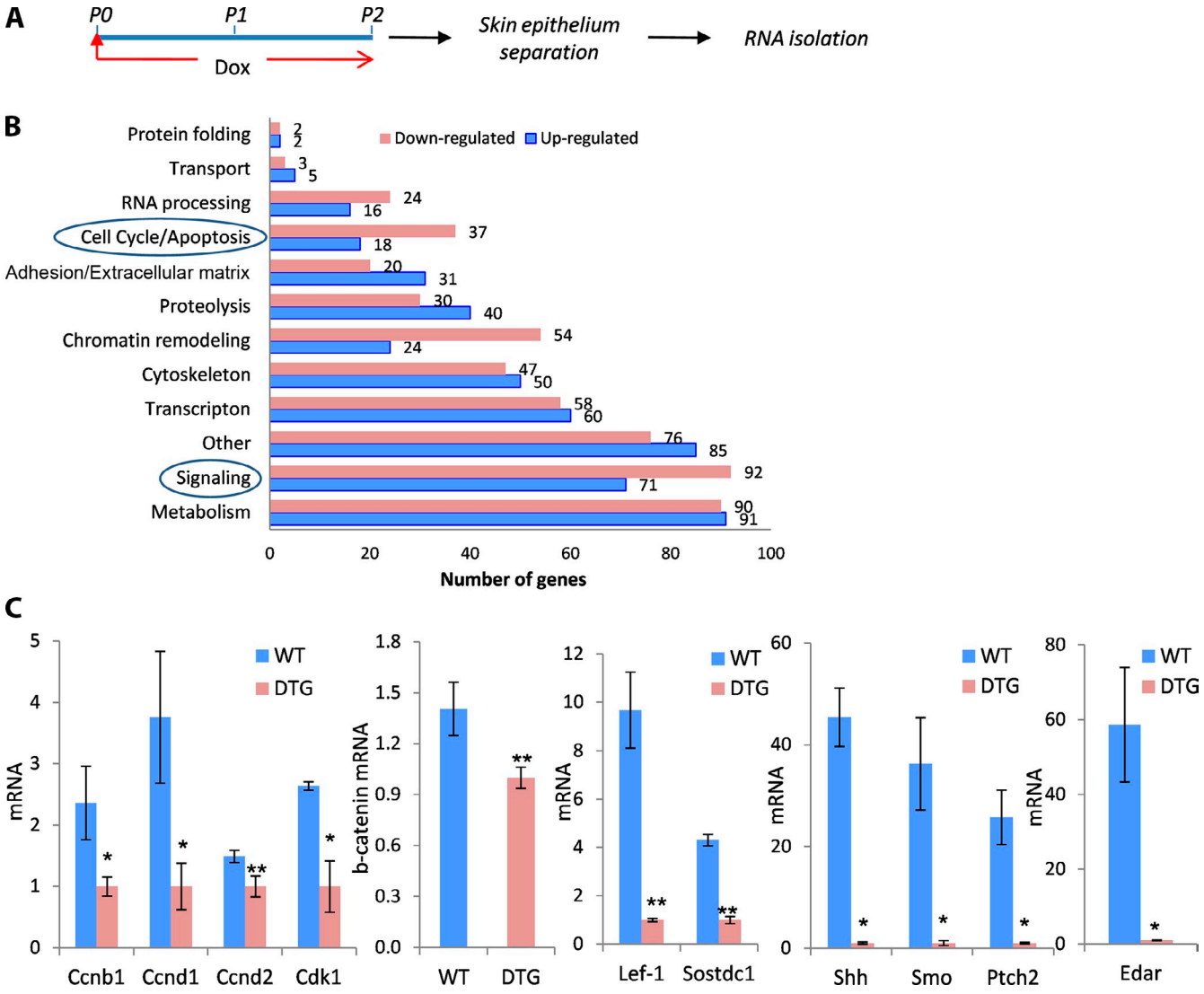

Figure 4. **Global gene expression profiling of the back skin epithelium of WT and K14-rtTA/miR-214-TRE mice.** (A) Schematic illustration of the experimental design. (B) Agilent microarray analysis of the back skin epithelium of DTG and WT mice. A bar chart depicts the ontology of the down- and up-regulated genes and the actual number of genes with more than twofold expression change in DTG and WT skin; (a full list of the genes is shown in Tables S1 and S2). (C) Validation of microarray. Real-time RT-PCR analysis of expression of the selected genes is shown. $n = 3$ mice/genotype. Data are presented as mean ± SD (error bars); *, $P < 0.05$; **, $P < 0.01$; Student's t test.

decreased levels of β-catenin, the downstream component of the Wnt pathway, in the HF placode epithelium of DTG mice (stages 1–2 of HF development; Fig. 5, A and H). Consistent with these data, a significant decrease of the β-catenin protein levels in the total skin of DTG mice was confirmed by Western blotting (Fig. 5 A). Lef-1 expression was also markedly decreased in the HF placode epithelium and in the developing dermal papilla (Fig. 5, B and H). In contrast, pSmad1/5/8 expression increased in the developing hair placodes and interfollicular epidermis of DTG mice versus WT controls, which suggests activation of BMP signaling driven by miR-214 overexpression (Fig. 5, C and H). Gain of miR-214 in the skin also resulted in the reduced expression of Shh (Fig. 5, D and I; and Fig. S1 F) and Edar (Fig. 5, D, E, and H). Analysis of Cyclin D1 and Cyclin D2 expression also revealed their decreased expression in the developing hair placodes (Fig. 5, F–H), as well as a reduced number of Cyclin D1–positive cells in the epidermis of DTG mice versus WT mice (Fig. S1 G). However, there were no changes in the expression of selected stem cell markers, such as Sox9 and Lhx2, between the hair placodes of DTG and WT mice (Fig. S1 H).

Similar to the HF development, elevation of miR-214 levels during hair cycle resulted in decreased expressions of β-catenin and Lef-1 in the hair matrix and the dermal papilla of DTG follicles, whereas Sox2 expression in the dermal papilla remained unchanged (Fig. 6, A, B, and G; and Fig. S1 I). Also, quantitative immunofluorescence analysis revealed increased expression of pSmad 1/5/8 in differentiating HF keratinocytes of DTG versus WT mice (Fig. 6, C and G). Shh expression was strongly decreased in the hair matrix of DTG HFs (Fig. 6, D and G). Consistent with microarray data, expression of cyclin D1 was also decreased in the hair matrix of DTG HFs (Fig. 6, E and G), and reduced expression of cyclin-dependent kinase 1 was also seen in the hair matrix of miR-214 transgenic mice (Fig. 6, F and G). In addition, expression of the

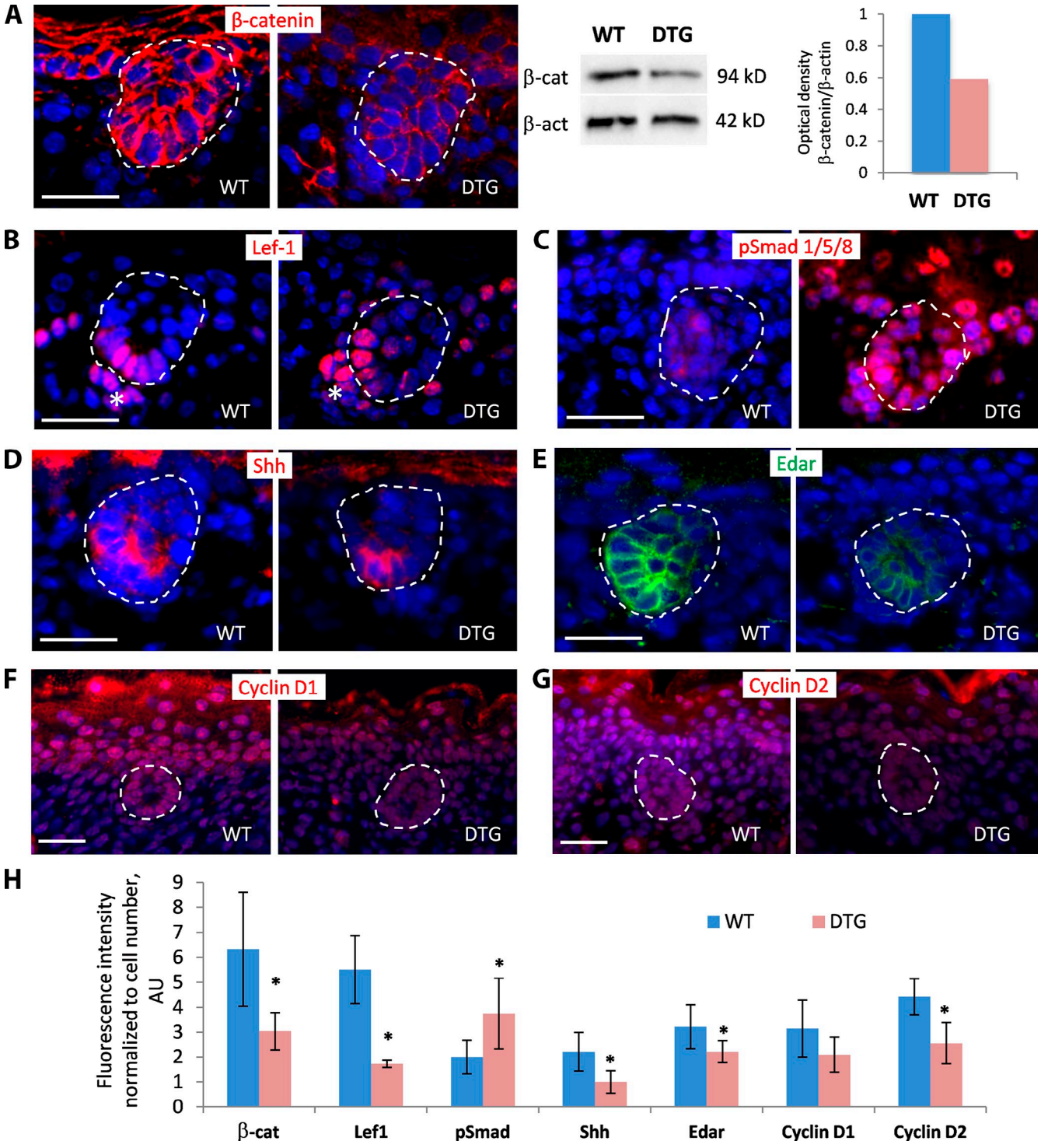

Figure 5. **Effect of miR-214 overexpression on the key regulators of HF morphogenesis.** (A, left) Immunofluorescence analysis of β-catenin (red) with nuclear staining (DAPI, blue). There was a marked decrease of β-catenin in hair placode epithelium of DTG mice at E17.5. (A, right) Western blot and its densitometry analysis. There were reduced levels of β-catenin protein in the skin of DTG mice at P0; data are shown as β-catenin band density normalized relative to β-actin. The data shown are from a single representative experiment out of three repeats. (B) Reduced expression of Lef-1 (red fluorescence) in hair placode epithelium and mesenchyme (asterisks) in the skin of DTG mice with nuclear staining (DAPI, blue). (C) More prominent expression of pSmad1/5/8 in DTG hair placodes and intrafollicular epidermis versus WT mice (red fluorescence; nuclear staining with DAPI, blue). (D and E) Decreased expressions of Shh (D) and Edar (E) in the HF placodes of DTG mice (red/green fluorescence; nuclear staining with DAPI, blue). (F and G) Reduced expression of Cyclin D1 (F) and Cyclin D2 (G) in the DTG hair placodes and the epidermis (red fluorescence; nuclear staining with DAPI, blue). (H) Quantitative immunofluorescence analysis. Immunofluorescence intensity was normalized to the number of DAPI+ cells in the selected areas. $n = 3$ mice/genotype. Data are presented as mean ± SD (error bars); *, $P < 0.05$; Student's *t* test. Broken lines demarcate the examples of the areas used for quantitative immunofluorescence analysis. Bars: (A–E) 25 µm; (F and G) 50 µm.

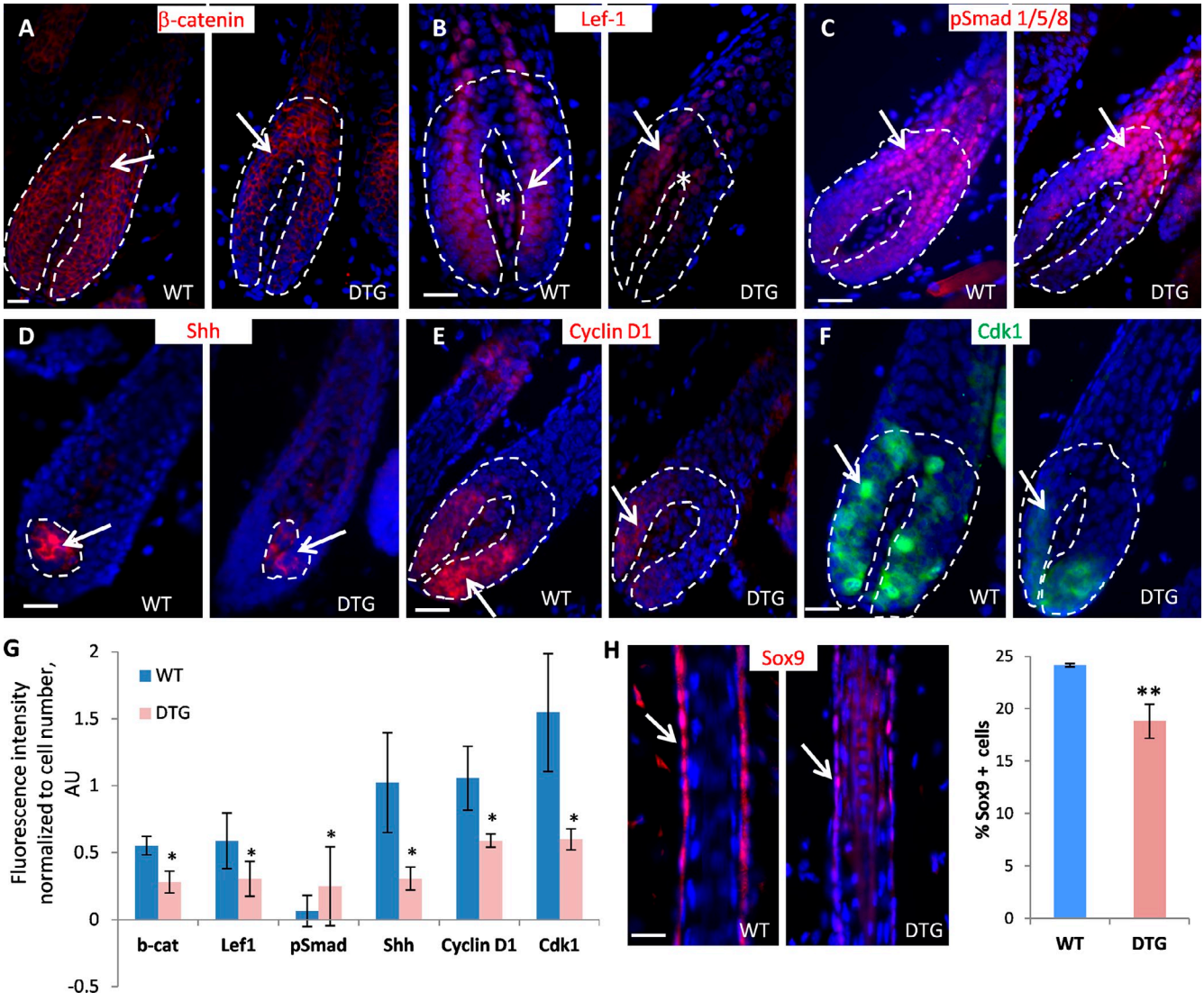

Figure 6. **Effect of miR-214 overexpression on the key regulators of HF cycling.** (A and B) Reduced expression of β-catenin and Lef-1 (red fluorescence) in the hair matrix (arrows) and dermal papilla (asterisks) of DTG follicles (nuclear staining with DAPI, blue). (C) Increased pSmad 1/5/8 expression in the postmitotic keratinocytes of the hair bulb and precortex in DTG mice (arrow; red fluorescence; nuclear staining with DAPI, blue). (D) Decrease in Shh expression in the hair matrix of DTG mice (arrow; red fluorescence; nuclear staining with DAPI, blue). (E and F) Decreased expression of cyclin D1 (red fluorescence) and cyclin-dependent kinase 1 (green fluorescence) in the hair matrix of DTG mice (arrows; nuclear staining with DAPI, blue). (G) Quantitative immunofluorescence analysis. Immunofluorescence intensity was normalized to the number of DAPI+ cells. n = 3 mice/genotype. The broken lines demarcate the areas of the examples used for quantitative immunofluorescence analysis. (H, left) Immunodetection of Sox9+ cells in the HF outer root sheath (red fluorescence). (H, right) Quantification of Sox9+ cells in the outer root sheath. n = 3 mice/genotype. Data are presented as mean ± SD (error bars); *, $P < 0.05$; **, $P < 0.01$; Student's t test. Bars: (A–F) 50 µm; (H) 25 µm.

Dlx3 transcription factor involved in the control of HF keratinocyte differentiation was less pronounced in transgenic HFs versus the controls (Fig. S1 J). Overexpression of miR-214 during the hair cycle was associated with a significant decrease in the number of Sox9-positive cells in the outer root sheath, which suggests a reduced supply of the progenitor cells from the bulge for the hair matrix of actively growing HFs upon miR-214 overexpression (Fig. 6 H).

These data suggest that miR-214 exerts inhibitory effects on HF development and cycling, at least in part, by regulating the activity of key signaling pathways (Wnt, Hedgehog, Bmp, and Edar) in keratinocytes, as well as by modulation of Wnt signaling in dermal papilla fibroblasts.

β-Catenin is a direct target of miR-214 in keratinocytes

To identify the direct targets of miR-214 in keratinocytes, gene expression profiling results obtained from the epithelium of neonatal DTG mice after 48 h of Dox activation were linked with four databases for prediction of miRNA targets, including PITA, miRanda, miRDB, and Targetscan (Rehmsmeier et al., 2004; Lewis et al., 2005; Kertesz et al., 2007; Wang and El Naqa, 2008; Fig. 7 A). The largest number of possible miR-214 target genes was predicted by PITA and miRanda (192 and 78, respectively), whereas TargetScan and miRDB showed only 18 and 11 possible targets, respectively. Intersections of PITA, miRanda, and miRDB predictions identified nine common

possible miR-214 targets, including *Ctnnb1* and *Shh* (Fig. S1 K). However, an overlap of all four databases revealed only three predicted target genes for miR-214, whose expression was altered in keratinocytes of DTG mice, including *Ctnnb1*, but not *Shh* (Fig. 7 A and Fig. S1 K).

To validate the results of bioinformatic analysis and explore whether *β-catenin* and *Shh* 3′ UTRs carry functional binding sites for miR-214 (Fig. 7 B and Fig. 1 L), the luciferase reporter assay was performed. Cotransfection of HaCaT cells with miR-214 mimic and the *β-catenin* 3′ UTR reporter construct caused significant reduction in luciferase activity, compared with the corresponding control, whereas this effect was not detected when *β-catenin* 3′ UTR was mutated (Fig. 7 C), thus confirming that *β-catenin* is a direct target of miR-214. However, the luciferase reporter assay did not confirm the direct interactions between miR-214 and 3′ UTR of *Shh*, which suggests that a decrease of its expression in the HFs after miR-214 overexpression is a secondary effect mediated by other factors (Fig. S1 M).

Next, the effect of miR-214 on the β-catenin/Tcf-dependent transcription activity was evaluated by using the TOPflash reporter assay. A significant induction in TOPflash reporter activity, without any effect on FOPflash activity (negative control), was detected in HaCaT cells treated with a synthetic Wnt agonist 6-bromoindirubin-3′-oxime (BIO; Meijer et al., 2003; Sato et al., 2004), whereas transfection of cells with miR-214 mimic significantly diminished TOPflash activity induced by BIO (Fig. 7 D).

Simultaneous in situ hybridization for miR-214 and immunofluorescence detection of β-catenin revealed a predominantly reciprocal expression pattern of miR-214 and β-catenin in the epidermis: miR-214 was seen in the suprabasal layer, whereas β-catenin was more strongly expressed in the basal cells (Fig. 7 E). A more complex pattern of miR-214 and β-catenin expressions was observed in the HFs: clear colocalization of miR-214 and β-catenin was seen in undifferentiated proliferating cells of the developing HFs and anagen hair matrix, whereas β-catenin was not coexpressed with miR-214 in the differentiating cells of the precortex (Fig. 7 E).

Furthermore, transfection of primary mouse epidermal keratinocytes (PMEKs) with either miR-214 mimic or its specific inhibitor resulted in the decrease and increase of the *β-catenin* mRNA expression, respectively (Fig. 7 F). Also, miR-214 mimic reduced levels of β-catenin protein in the keratinocytes (Fig. 7 G). miR-214 was also capable of interfering with the activity of Wnt signaling in keratinocytes induced by the GSK-3β inhibitor lithium chloride (LiCl; Klein and Melton, 1996; Fig. 7 H). Immunofluorescence analysis confirmed that miR-214 mimic decreases nuclear and cytoplasmic β-catenin protein levels compared with the control. Moreover, miR-214 abrogated LiCl-induced β-catenin expression: both nuclear and cytoplasmic β-catenin levels were significantly decreased in the keratinocytes synergistically treated with LiCl and miR-214 mimic compared with the cells treated with LiCl alone (Fig. 7 H). Consistent with this observation, Western blot analysis showed reduced levels of β-catenin in the keratinocytes cotreated with LiCl and miR-214 mimic compared with the cells treated with LiCl solo (Fig. S1 N).

Collectively, these data suggest that β-catenin is a genuine target of miR-214, and that miR-214 is involved in the control of the activity of the Wnt pathway in keratinocytes.

Activation of Wnt signaling rescues the skin phenotype in miR-214 transgenic mice

To further explore the functional links between miR-214 and β-catenin in vivo, miR-214 transgene was induced after E10.5, followed by the subcutaneous injections of Wnt agonist BIO on five consecutive days after birth. Although β-catenin mRNA levels were low in the skin of DTG mice treated with BIO, β-catenin protein expression was quite similar in the HFs of DTG and WT mice (Fig. 8, A and B). This suggests that the reduced levels of the β-catenin transcript were most likely compensated by β-catenin protein stabilization caused by the GSK-3 inhibition induced by BIO (Meijer et al., 2003). Pharmacological experiments revealed that BIO treatment lead to induction of new HFs in DTG mice postnatally, which resulted in the appearance of the HFs at early stages of morphogenesis (stages 2–3) in DTG mice followed by restoration of their total number, similar to the WT controls (Fig. 8, C–E). In addition, pharmacological Wnt activation resulted in a significant increase of the hair bulb diameter in the HFs at advanced stages (stages 6–7) of morphogenesis in DTG mice, whereas no increase of the hair bulb size was seen in WT mice treated with BIO (Fig. 8 F). These observations demonstrate that activation of Wnt signaling in DTG mice rescues the effects of miR-214 overexpression in vivo, confirming further that miR-214 does indeed interfere with Wnt pathway activity in the developing and postnatal skin.

Discussion

MicroRNA-dependent control of gene expression plays a fundamental role in the balancing and fine-tuning of lineage-specific differentiation programs in many organs, including skin (Andl et al., 2006; Yi et al., 2006). In this paper, we identify a novel role for miR-214 in the control of skin and HF development, and demonstrate that: (1) miR-214 shows spatial-temporal changes in the expression pattern in the skin during HF morphogenesis and cycling; (2) inducible overexpression of miR-214 in keratinocytes inhibits cell proliferation, and results in a formation of fewer HFs with decreased size of the hair bulb, which produce thinner hair; (3) miR-214 regulates the balance in the activities of multiple signaling pathways, including Wnt, Shh, Edar, and Bmp, in developing and postnatal skin; and (4) β-catenin serves as a direct miR-214 target in keratinocytes.

During skin development and postnatal growth, miR-214 expression predominates in differentiating populations of keratinocytes committed either to epidermal or HF cell fates (suprabasal epidermal or hair matrix keratinocytes, respectively), whereas its expression in the progenitor cell populations of the basal epidermal layer or HF outer root sheath appears to be considerably lower. K14-driven miR-214 overexpression in the progenitor cell populations of the epidermis and HF results in a reduced epidermal proliferation and accelerated differentiation,

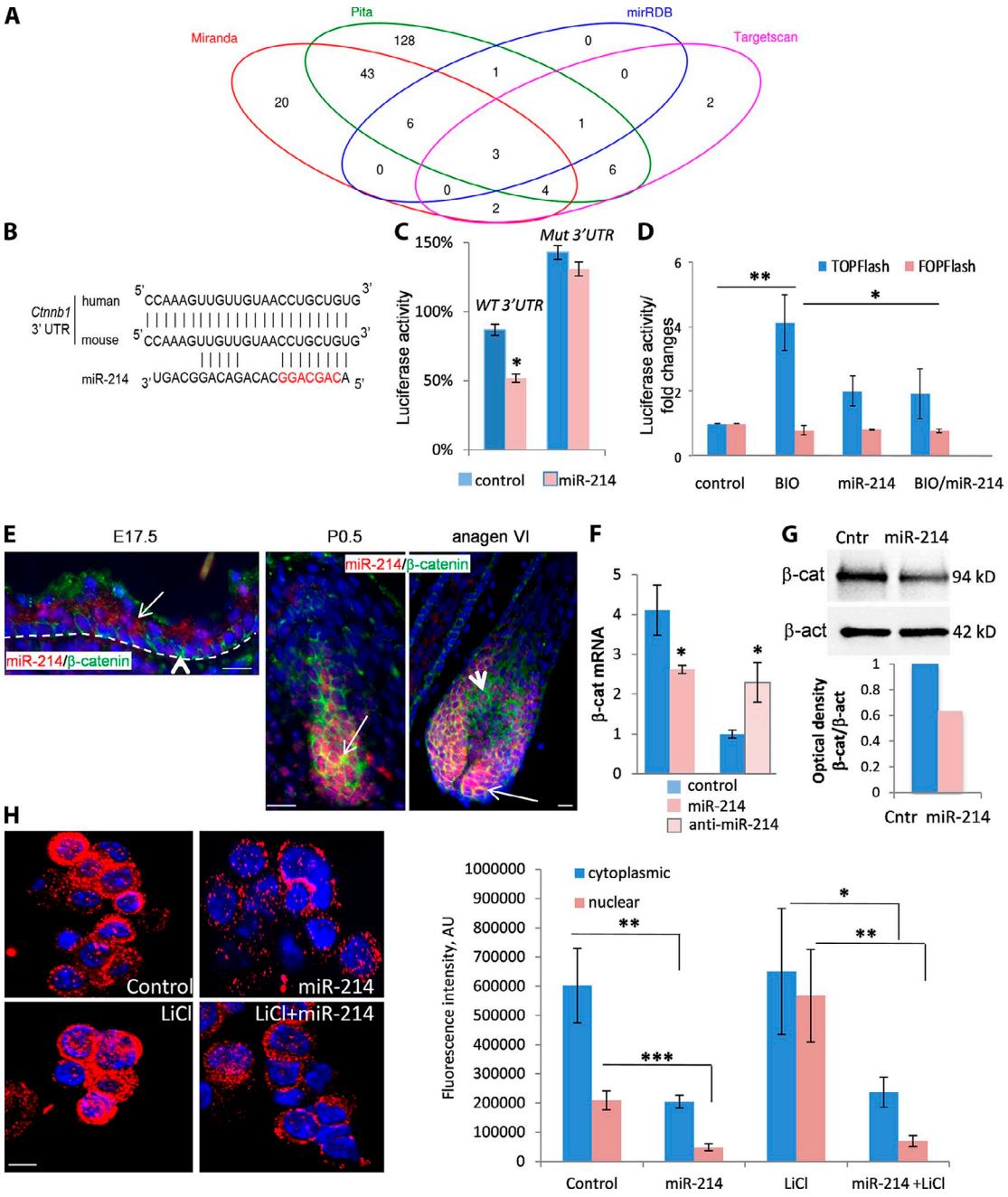

Figure 7. **miR-214 modulates the activity of Wnt signaling by targeting β-catenin.** (A) A Venn diagram depicting the overlap of four databases for prediction of miR-214 targets (PITA, miRanda, miRDB, and Targetscan) with gene expression profiling in the epithelium of neonatal DTG and WT mice after 48 h of Dox treatment. Only down-regulated genes (<1.5-fold) were included in the analysis. (B) Predicted interactions between miR-214 and *Ctnnb1*. Alignment of mouse and human sequences in the 3′ UTR of *Ctnnb1* mRNA is shown. (C) Significant reduction in luciferase activity in HaCaT cells due to cotransfection with miR-214 mimic and the *Ctnnb1* 3′ UTR construct encompassing the putative miR-214 target site. No changes in luciferase activity were detected when the miRNA binding site was mutated (mut-3′UTR). Each sample was normalized to Renilla luciferase activity. The data shown are from a single representative experiment out of three repeats. For the experiment shown, $n = 3$ for all experimental conditions. (D) TOPflash reporter assay. There was significant induction in TOPflash reporter activity in HaCaT cells by BIO, which was diminished by miR-214 mimic. There were no changes in FOPflash activity in any experimental groups. The data shown are from a single representative experiment out of three repeats. For the experiment shown, $n = 3$. (E) Dual fluorescent in situ hybridization for miR-214 (red) and immunofluorescence of β-catenin (green). β-Catenin is expressed in the basal layer (arrowhead), while more prominent miR-214 expression was seen in the suprabasal cells of the E17.5 epidermis (arrow). There was coexpression of miR-214 and β-catenin in the developing HF (stage 3 morphogenesis) and anagen VI hair matrix (arrows). There was also a lack of miR-214 in β-catenin+ differentiating cells of the precortex (arrowhead). The broken line demarcates the epidermal–dermal border. (F) Real-time RT-PCR. β-Catenin expression in primary epidermal keratinocytes transfected with either miR-214 mimic or miR-214 inhibitor is shown. The data shown are from a single representative experiment out of three repeats. For the experiment shown, $n = 3$. (G) Western blot and its densitometry analysis. There were reduced levels of β-catenin protein in primary epidermal keratinocytes transfected with miR-214 mimic. Data are shown as β-catenin band density normalized relative to β-actin. The data shown are from a single representative experiment out of three repeats. (H) Immunocytochemistry and quantitative immunofluorescence. There was prominent β-catenin staining (red) in primary epidermal keratinocytes treated with the GSK-3β inhibitor LiCl compared with the control, and decreased β-catenin staining in the nucleus of keratinocytes transfected with miR-214 mimic and synergistically exposed to miR-214 mimic and LiCl. The data shown are from a single representative experiment out of three repeats. For the experiment shown, $n = 3$. Data are presented as mean ± SD (error bars); *, $P < 0.05$; **, $P < 0.001$; ***, $P < 0.0001$; Student's *t* test. Bars: (E) 50 µm; (H) 5 µm.

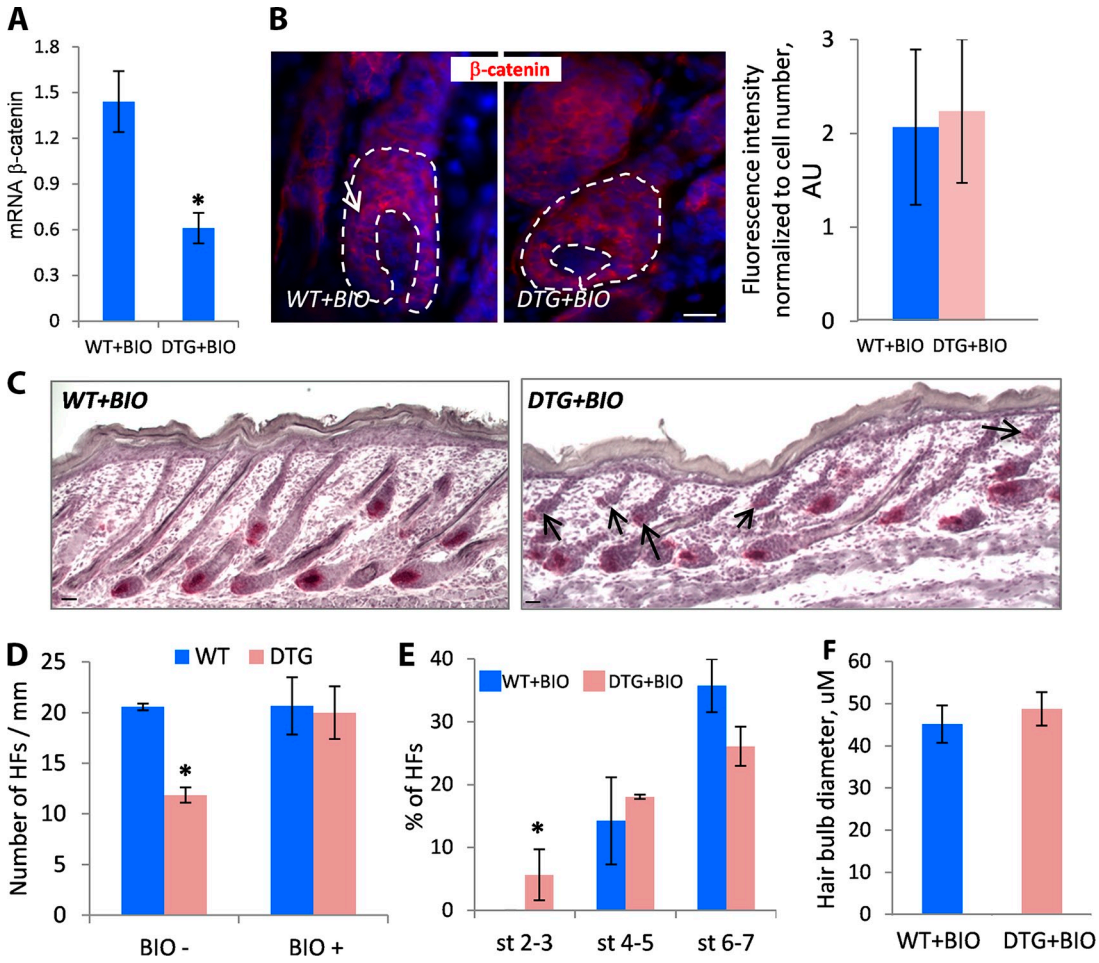

Figure 8. **Activation of Wnt signaling rescues the skin phenotype in miR-214 transgenic mice.** (A) Real-time RT-PCR. There were decreased levels of *β-catenin* transcript in the DTG skin treated with BIO versus BIO-treated WT mice. *n* = 3 mice/genotype. (B) Immunofluorescence analysis of β-catenin (red) in the HFs of WT and DTG mice treated with Wnt agonist BIO on 5 consecutive days (arrow). The broken lines demarcate the examples of the areas used for quantitative immunofluorescence analysis. Bar, 25 µm. (C) Representative microphotographs of back skin histology of WT and DTG mice after 5 d of BIO treatment at P5.5. Arrows show HF at 2–3 stages of morphogenesis. Bar, 100 µm. (D) There was a significant reduction in the number of HFs in DTG versus WT littermate at P5.5, while there was no difference in HF number between WT and DTG mice after 5 d of BIO treatment. Bar, 50 µm. *n* = 3 mice/genotype. (E) Quantitative analysis of HF at different stages of morphogenesis in the skin of WT and DTG mice after 5 d of BIO treatment. *n* = 3 mice/genotype. (F) Histomorphometric analysis of hair bulb diameter in DTG and WT skin treated with BIO as measured across the widest part. *n* = 3 mice/genotype. Data are presented as mean ± SD (error bars). *, P < 0.05; Student's *t* test.

as well as in formation of ∼30% fewer HFs with decreased hair bulb size and producing thinner hairs.

Skin and HF morphogenesis is controlled by coordinated activities of the Wnt, Hedgehog, Edar, Bmp, Fgf, Notch, and other signaling pathways (Millar, 2002; Schmidt-Ullrich and Paus, 2005; Blanpain and Fuchs, 2009). Among these pathways, Wnt signaling operates as the most powerful regulator of skin development. It controls cell proliferation in both epithelium (epidermis, HF matrix) and mesenchyme, and regulates differentiation of hair matrix keratinocytes and the morphogen-producing activity of dermal papilla cells (Zhou et al., 1995; Huelsken et al., 2001; Andl et al., 2002; Enshell-Seijffers et al., 2010; Choi et al., 2013; Fu and Hsu, 2013; Tsai et al., 2014). In the developing HFs, the Wnt signaling pathway operates as the activator of the placode formation, whereas BMP signaling inhibits this process and, together with Wnt inhibitors, Dkk1/2/4 promotes the interplacode cell fate in the epidermal progenitor cells (Botchkarev et al., 1999; Jiang et al., 1999; Andl et al., 2002; Sick et al., 2006). In turn, FGF and Edar pathways promote the placode cell fate, at least in part, by inhibiting the activity of BMP signaling (Eivers et al., 2008; Plouhinec et al., 2011), whereas Edar via the NF-kB pathway stimulates expression of the BMP antagonists, such as connective tissue growth factor (CTGF) and Follistatin (Mou et al., 2006). Edar serves as a downstream effector of Wnt signaling, which is initially activated in preplacodes independently of Edar/NF-κB activity, whereas later Edar signaling is required to refine the pattern of Wnt/β-catenin activity via stimulation of expression of the Wnt10b in the placode progenitor cells (Zhang et al., 2009). In addition, Edar signaling promotes HF placode formation by stimulation of Sonic hedgehog expression (Pummila et al., 2007), which operates as a potent stimulator of keratinocyte proliferation in the developing HF (St-Jacques et al., 1998; Chiang et al., 1999).

Recent data suggest that the activity of the Wnt signaling pathway varies considerably in distinct skin compartments:

low levels of activity are required for maintenance of epidermal proliferation, medium level signaling is required for maintenance of epithelial–mesenchymal interactions in the hair bulb to promote active hair growth phase, and high activity promotes hair shaft differentiation (Choi et al., 2013). Our data demonstrate that miR-214 contributes to the regulation of the activity of Wnt signaling in the developing and postnatal skin, at least in part, by targeting its key component β-catenin: (1) miR-214 and β-catenin exhibit reciprocal expression pattern in the epidermis, whereas miR-214 and β-catenin are colocalized in undifferentiated epithelial cells of the hair peg and in hair matrix keratinocytes; (2) β-catenin expression is markedly decreased in the epidermis, HF placodes, HF matrix, and dermal papilla after K14-driven miR-214 overexpression; (3) bioinformatic prediction analysis and experimental data confirms direct targeting of *β-catenin* 3′ UTR by miR-214 in keratinocytes; and (4) miR-214 is capable of interfering with the activity of Wnt signaling after its activation by the GSK-3β inhibitors both in vitro and in vivo.

Furthermore, the skin phenotype of miR-214 transgenic mice (decreased epidermal proliferation, proportional decrease in the number of all HF types, decrease of the size of hair bulbs, and formation of thinner hair versus the corresponding WT controls) is consistent with the skin phenotype of mice with conditional ablation of β-catenin either in keratinocytes or in the dermal papilla fibroblasts (Huelsken et al., 2001; Enshell-Seijffers et al., 2010; Tsai et al., 2014). Importantly, the key features of the skin phenotype in miR-214–overexpressing mice (decrease of the HF number and hair bulb size) are rescued by pharmacological activation of the Wnt pathway in vivo, thus further supporting the links between miR-214 and Wnt pathway activity in the skin. These data are also consistent with data published previously showing miR-214 targeting of β-catenin in hepatocellular carcinoma cells (Wang et al., 2012).

The Wnt signaling pathway is a potent regulator of cell proliferation, and many effects of miR-214 on skin and HF development are most likely associated with interference with cell cycle regulation: indeed, short-term activation of miR-214 (48 h) suppressed the expressions of several cyclins and cyclin-dependent kinases, including *cyclin B*, *cyclin D1*, *cyclin D2*, and *cdk1*. Consistent with these observations, substantial up-regulation in the cyclin-dependent kinase inhibitors p16 and p19 was still detected in fully developed follicles of the K14rtTA/TRE-miR-214 mice, which suggests the activation of the anti-proliferative program in response to increased levels of miR-214 in the keratinocytes. These data are in line with the results obtained in other models demonstrating that miR-214 expression is substantially decreased in cutaneous squamous cell carcinoma (Yamane et al., 2013) and that the anti-proliferative effects of miR-214 in the myoblast cell line are achieved by targeting Nras (Liu et al., 2010).

Reduced cell proliferation seen in the epidermis and HFs in K14rtTA/TRE-miR-214 mice could also be a result of altered activity of Shh signaling. Indeed, K14rtTA/TRE-miR-214 mice showed decreased expression of Shh and its signal tranducer Smo. Shh signaling is required for post-hair placode initiation growth by stimulating proliferation of HF epithelial cells via transcriptional activation of cyclin D1 and cyclin D2 (St-Jacques et al., 1998; Chiang et al., 1999; Mill et al., 2003; Schmidt-Ullrich et al., 2006). Shh also promotes epidermal proliferation (Zhou et al., 2006). In adult mice, Shh is essential for anagen onset and proper hair cycling (Sato et al., 1999; Wang et al., 2000). However, our experimental data validating the bioinformatic prediction suggested that *Shh* does not serve as a direct miR-214 target in the keratinocytes. Given that Wnt signaling operates as upstream of Edar and Shh pathways in the control of the HF placode formation (Schmidt-Ullrich et al., 2006; Zhang et al., 2009), these data suggest that down-regulation of Edar and Shh expression seen in the HF placodes of miR-214 DTG mice is, most likely, a result of the indirect effects linked to the miR-214–mediated decrease of Wnt signaling activity in keratinocytes.

Our data demonstrating that overexpression of miR-214 results in the development of smaller HFs producing thinner hair suggest miR-214 involvement in the control of HF size and its relevance to the mechanisms that contribute to HF miniaturization seen in androgenetic alopecia (Garza et al., 2011). However, additional studies are required to assess the role of miR-214 in the control of HF size in human skin, as well as the potential involvement of miR-214 in regulation of the activity of distinct HF stem cell populations residing in secondary hair germ and bulge during hair cycle (Hsu et al., 2011; Rompolas and Greco, 2014). Our data suggest that the decrease of HF size in K14rtTA/TRE-miR-214 mice could not only be associated with the decreased proliferation in the hair matrix, but also with miR-214 effects on the migration of the progenitor cells from the bulge alongside the outer root sheath toward the hair matrix.

Indeed, K14rtTA/miR-214 HFs contained significantly fewer Sox9+ cells in the outer root sheath. Sox9 is a transcriptional regulator that is expressed in the HF stem cells and their outer root sheath progenies, and is required for guiding stem cell progenies to the hair matrix (Vidal et al., 2005). Therefore, a reduced number of Sox9+ cells in the transgenic follicles suggests the inhibitory action of miR-214 on stem cells and their progenies, which contributes to the formation of the smaller hair bulbs. However, these effects could also be associated with decreased β-catenin expression, as β-catenin is acting as the upstream regulator of Sox9 expression in the intestinal epithelium and neural crest cells (Blache et al., 2004; Liu et al., 2013).

In addition to the changes seen in the HF epithelium, a significant reduction in the number of dermal papilla cells was observed in K14rtTA/miR-214 mice. This is consistent with previously published data demonstrating that a decrease of the hair bulb size is associated with reduced cellularity of the dermal papilla (Chi et al., 2013). Similar to mice with conditional ablation of β-catenin in the HF mesenchyme (Enshell-Seijffers et al., 2010), miR-214 overexpression results in the decrease of β-catenin, Lef1 expression, and lack of changes in Sox2 in the dermal papilla. Therefore, the effects seen in K14rtTA/miR-214 mice could be a result of the altered epithelial–mesenchymal interactions. Also, given that miRNAs are capable of exerting paracrine effects on distantly located cellular targets (Zhu and Fan, 2011), additional studies are required to clarify whether miR-214 overexpression in keratinocytes could directly influence

cell number and gene expression in dermal papilla fibroblasts, or if other paracrine factors released from keratinocytes affect traffic of the connective tissue progenitor cells to populate dermal papilla and/or their activity in the HFs in K14rtTA/miR-214 mice.

Additional studies are also required to define the upstream regulators that control miR-214 expression in the different cell types in the skin. For example, it has previously been shown that Twist1 transcriptionally regulates miR-214 expression in specific neural cell populations (Lee et al., 2009); however, a role of Twist1 in skin development and HF cycling remains unknown and needs to be carefully explored. Identification of the miR-214 upstream regulators in skin will help to recognize novel players in the miRNA-mediated gene regulatory circuits controlling keratinocyte proliferation and differentiation in the developing and postnatal skin.

In summary, our data reveal that miR-214 is a key determinant that controls the activity of the Wnt signaling pathway and β-catenin expression in the developing and postnatal skin and HFs. Because Wnt signaling plays a crucial role in the control of stem cell activity in many organs during development and regeneration, while its uncontrolled activation results in tumorigenesis (Chan et al., 1999; Malanchi et al., 2008), these data provide an important foundation for further analyses of the role of miR-214 as a regulator of Wnt pathway activity in many areas of research, including stem cell and cancer biology, regenerative medicine, and aging.

Materials and methods

Generation of transgenic mice

Animal studies were performed under protocols approved by Boston University and Home Office Project License (UK). K14-rtTA/TRE-miR-214 mice were generated on an FVB background. To generate TRE-miR-214 construct, a DNA fragment containing the precursor-mmu-miR-214 coding sequence was isolated from pCMV-miR-214 plasmid DNA (SC400919; OriGene) followed by blunt-end ligation into the pSTblue-1 vector (EMD Millipore). This fragment was then excised and ligated into BamHI–SalI sites of the pTRE2-Dual 2 plasmid (Takara Bio Inc.), which contains a pTight promoter consisting of a modified minimal CMV promoter, and seven direct repeats of a 36-bp regulatory sequence that contains the 19-bp tet-operator sequence, mCherry, and an internal ribosome entry site (IRES2). All cloning was verified by sequencing. A PspxI fragment from TRE-miR-214 construct was purified and pronuclear injections were performed in the Transgenic Core at the Boston University School of Medicine using FVB/NJ mice as a genetic background. Founders were identified by PCR using transgene promoter–specific DNA primers: forward, 5′-GTTCATGTACGGCTCCAAG-3′; and reverse, 5′-CGCAGCTTCACCTTGTAG-3′. To generate double-transgenic K14-rtTA/TRE-miR-214 mice, TRE-miR-214 mice were crossed with K14-rtTA according to standard protocols. To activate expression of tet/Dox-responsive transgenes, mice were fed chow containing 625 mg Dox/kg chow (Harlan Laboratories, Inc.). For activation of Wnt signaling, BIO (R&D Systems) was administered subcutaneously to back skin of neonatal mice in a concentration 2 µg/g (Gunn et al., 2011; Kwon et al., 2014) during five constitutive days starting from day 0 after birth.

Genotyping

Genotyping was performed using the following primers and PCR parameters. For K14rtTA mouse genotyping, primer sequences used were provided by The Jackson Laboratory, including forward primer oIMR7862, 5′-CACGATACACCTGACTAGCTGGGTG-3′; and reverse primer oIMR7863, 5′-CATCACCCACAGGCTAGCGCCAACT-3′ (PCR parameters: 94°C for 3 min [94°C for 30 s, 67°C for 60 s, 72°C for 60 s] for 35 cycles, 72°C for 2 min). For TRE-miR-214 mice, the forward primer, 5′-AGAACGTATGTCGAGGTAG-3′; and reverse primer, 5′-TTGGAGCCGTACATGAAC-3′ were used (PCR parameters: 94°C for 3 min [94°C for 30 s, 67°C for 60 s, 72°C for 60 s] for 35 cycles, 72°C for 2 min).

In situ hybridization, immunofluorescence, and histology

Skin cryosections (10 µm) were fixed in 4% paraformaldehyde for 10 min at room temperature. In brief, tissue sections were acetylated in triethanolamine buffer (4.5 mM triethanolamine, 6 M NCl, and 3 mM acetic anhydride) for 10 min and permeabilized (1% Triton X-100/1× DEPC-treated PBS) for 30 min, slides were hybridized with 2.5 pmol DIG-labeled miR-214 probe (Exiqon) diluted in hybridization buffer (50% formamide DI, 2× saline-sodium citrate (SCC), 1% dextran sulfate, and 0.4 mg/ml tRNA) for 16–18 h at 55°C overnight. Slides were subsequently washed twice in SCC (10 min, 4 times, 65°C), 0.1× SCC (60 min, 65°C), and 0.2× SCC (10 min, RT). Immunodetection of miR-214 was performed with sheep alkaline phosphatase–conjugated anti-DIG antibody (1:5,000; Roche) followed by a staining reaction with NBT/BCIP solution (Roche) for 16–18 h at RT. Alternatively, the signal was developed with the Tyramide Signal Amplification (TSA) system with FITC-conjugated reagent (PerkinElmer).

For immunofluorescence, the formalin-fixed cryosections or methanol-fixed cells were incubated with primary antisera listed in Table 1 overnight at 4°C, followed by application of corresponding Alexa Fluor 555 or Alexa Fluor 488 antibodies (1:200; Invitrogen) for 45 min at 37°C. Incubation steps were interspersed by washes with PBS. Sections were counterstained with DAPI.

For dual fluorescent in situ hybridization and immunofluorescence developed with the TSA system, in situ hybridization slides were processed for β-catenin immunofluorescence as described in the previous paragraph. For double immunofluorescence of Keratins and BrdU, the slides were treated with DNase I (20 µg/ml; Sigma-Aldrich) for 2 h at 37°C, then incubated with primary antibodies against BrdU (1:500; Abcam), followed by subsequent antibody costaining as described in the previous paragraph.

For detection of endogenous alkaline phosphatase, acetone-fixed cryosections (10 µm) were incubated in developing solution (100 mM NaCl, pH 8.3, 100 mM Tris, pH 9.5, 20 mM HCl, 0.05% Naphtol ASBI phosphate, 0.5% DMF, 25 mM sodium-nitrite, and 5% New fuchsin) for 15 min, followed by a quick wash in PBS and immersion of the slides in Vector Hematoxylin Nuclear counterstain solution (Vector Laboratories) for 30 s at RT (Botchkareva et al., 1999; Paus et al., 1999).

Microscopy and image analyses

Images were taken at RT using the fluorochromes DAPI, Alexa Fluor 488 (green), and Alexa Fluor 555 (red). Fluorescence images were acquired with a microscope (Eclipse50i) equipped with a Plan Fluor 20×/0.50 NA or 40×/0.75 NA objective lens (Nikon), a camera (EXi Aqua; QImaging), and Image-Pro Express software (version 6.3; Media Cybernetics). Brightfield microscopy was performed using a microscope (Eclipse 50i; Nikon) equipped with a Plan Fluor 20×/0.50 NA or 40×/0.75 NA objective lens (Nikon), a camera (VisiCam 3.0; VWR International), and Visi-Cam Image Analyzer software (VWR International). No imaging medium was used. For the illustration purposes, images of the skin cryosections were adjusted using the levels and brightness/contrast tools in Photoshop (CS6; Adobe); the same adjustments were applied to every pixel in each RGB channel.

Microarray and real-time PCR

Newborn K14-rtTA/TRE-miR-214 and WT mice were treated with Dox for 48 h to induce miR-214 followed by skin harvesting. Skins were treated with dispase at 37°C for 30 min to collect epidermis and HF epithelium. Total RNA was isolated by TRIzol (Sigma-Aldrich) and processed for microarray analysis by using 41K Whole Mouse Genome 60-mer oligo-microarray (Agilent Technologies). Expression of miR-214 was determined using TaqMan real-time PCR Assay (Applied Biosystems) under the following cycling conditions: 95°C for 10 min, followed by 40 cycles of 95°C for 15 s and 60°C for 60 s.

Differences between samples and controls were calculated based on the Ct ($^{\Delta\Delta}$Ct) method and normalized to the small nucleolar RNA 202 values (SnoRNA). Data were pooled, the means ± SD were calculated, and statistical analysis was performed using an unpaired Student's *t* test. Quantitative RT-PCR for mRNA was performed with iQ SYBR Green Supermix (Bio-Rad Laboratories), using 10 ng cDNA and 1 µM primers. PCR primers were designed with Beacon Designer software (Premier Biosoft International; Table 2). Amplification was performed at the following conditions: 95°C for 5 min, followed by 40 cycles of denaturation (95°C for 15 s), annealing (30 s at temperature experimentally determined for each primer pairs), and elongation (72°C for 15 s). Data analysis was performed as described above. Differences between samples and controls were calculated based on the Ct ($^{\Delta\Delta}$Ct) method and normalized to *β-actin*. Statistical analysis was performed using an unpaired Student's *t* test.

Table 1. **Primary antibodies and associated dilutions**

Antibody	Host	Dilution	Source
β-Catenin	Rabbit	1:2,000	Abcam
BrdU	Sheep	1:100	Abcam
CD34	Goat	1:200	BD
Cyclin D1	Rabbit	1:100	Abcam
Cyclin D2	Rabbit	1:100	Abcam
Cdk1	mouse	1:100	Abcam
Cytokeratin 10	Rabbit	1:500	Abcam
Cytokeratin 14	Guinea pig	1:500	Acris
Dlx3	Goat	1:500	Santa Cruz Biotechnology, Inc.
Edar	Goat	1:500	R&D Systems
Ki67	Rabbit	1:100	Abcam
Lef-1	Rabbit	1:100	Cell Signaling Technology
Lhx2	Goat	1:200	Santa Cruz Biotechnology, Inc.
Loricin	Rabbit	1:100	Abcam
Phospho-H3	Rabbit	1:100	Cell Signaling Technology
Phospho-Smad 1/5/8	Rabbit	1:500	Abcam
Sox 2	Goat	1:200	Santa Cruz Biotechnology, Inc.
Sox 9	Rabbit	1:250	Santa Cruz Biotechnology, Inc.
Shh	Rabbit	1:100	Santa Cruz Biotechnology, Inc.

Western blot analysis

5 µg of protein was extracted from snap-frozen skin samples or cultured cells with lysis buffer consisting of 50 mm Tris-HCl, 1% NP-40, 0.25% sodium deoxycholate, 150 mm NaCl, 1 mm EDTA, pH 7.4, and Complete Ultra protease inhibitor cocktail (Roche). Protein concentrations were determined using the Bradford assay. Proteins were resolved via SDS-PAGE. Membranes were incubated with primary antibodies against β-catenin (1:2,000) and β-actin (1:2,000; Table 1) overnight at 4°C. Horseradish peroxidase-tagged IgG antibody was used as a secondary antibody (1:5,000; Thermo Fisher Scientific). Antibody binding was visualized with an enhanced chemiluminescence system (SuperSignal West Pico kit; Thermo Fisher Scientific) and the Gel Doc XR+ system (Bio-Rad Laboratories). Densitometric analysis was performed using ImageJ software (National Institutes of Health).

Histomorphometry, quantitative immunofluorescence, and statistical analysis

For histomorphometry analysis, every tenth cryosection of dorsal skin from K14-rtTA/TRE-miR-214 and WT mice was used to exclude the repetitive evaluation of the same HF. The number of HFs per millimeter of epidermal length was calculated using sections from dorsal skin of K14-rtTA/TRE-miR-214 and WT samples at the different developmental points, including E17.5, P0.5, and P8.5.5 (n = 3 per each experimental group). Proliferation in the epidermis was assessed by the calculation of the ratio of the number of Ki67+ cells to DAPI+ cells in 50–60 microscopic fields. Proliferation in the HF was assessed by calculating the ratio of pH3(Ser28)+ to DAPI+ cells per hair bulb in 50–60 HFs of either K14-rtTA/TRE-miR-214 or WT mice. The hair bulb diameter was measured across the widest part of the bulb (Auber line). Altogether, HFs in 50–60 microscopic fields from distinct time points were analyzed and compared with a corresponding number of HF from the appropriate age-matched WT mice. Comparative analysis of Sox9+ cells was done by evaluating the ratio of the number Sox9+ to DAPI+ cells in the outer root sheath (from the distal end of the bulb to the sebaceous duct). In total, 50–60 follicles of either WT or K14-rtTA/TRE-miR-214 mice were included in the analysis. Data were pooled, the means ± SD were calculated, and statistical analysis was performed using an unpaired Student's t test.

For the assessment of the hair shaft length and width of the four HF types (guard, awl, auchene, and zigzag), hairs were plucked from the back skin of K14rtTA/TRE-miR-214 (n = 4) and WT mice (n = 4) in the telogen

Table 2. **List of primers used for RT-qPCR**

Gene		Accession	Sense sequence (5′-3′)	Anti-sense sequence (5′-3′)
Axin	Axin2	NM_015732	CACCTCTCCTCTGTTACCTTC	GTCAACGCTCTGCCCTAC
Actb	Actin, β	NM_007393	TTCCAGCCTTCCTTCTTG	GGAGCCAGAGCAGTAATC
Ctnnb1	Catenin, β1	NM_001165902	GCCACCAAACAGATACATAC	CCTCTCAGCAACTCTACAG
Cdkn2a	Cyclin-dependent kinase inhibitor 2A	NM_009877	GCTCTTTGTGTTCCGCTG	CTCTGCTCTTGGGATTGG
Cdkn2d	Cyclin-dependent kinase inhibitor 2D (p19)	NM_009878	GGCTCCTACAGGCAACAG	TAGATGGCTCACACTTCAGG
Ccnd1	Cyclin D1	NM_007631	GAGACCATTCCCTTGACTGC	GAAATGAACTTCACATCTGTGGC
Ccnd2	Cyclin D2	NM_009829	GGATGCTAGAGGTCTGTGAGG	CCAACACTACCAGTTCCCAC
Ccnb1	Cyclin B1	NM_172301	ATAATCCCTCTCCAAGCCCG	CTGCTCTTCCTCCAGTTGTC
Cdk1	Cyclin-dependent kinase 1	NM_007659	ATCAGACTTGAAAGCGAGGA	GGTGTAAGTAACTCTTAACGAGTG
Edar	Ectodysplasin-A receptor	NM_010100	GCCCCACCGAGTTGCCGTTT	CCAGCCGCTCGATCTGCACC
Krt10	Keratin 10	NM_010660	AGTCTGAAATCACTGAATTG	ATCTGGCTTTGAATCTGG
Lef-1	Lymphoid enhancer binding factor 1	NM_001276402	ACTCCAAGCAAGGCATGTC	GGGTGATCTGTCCAACGC
Lor	Loricrin	NM_008508	TTCCAAACCCTTCACATTTTAAG	GGGAGGTAGTCATTCAGAAAC
Ptch2	Patched homologue 2	NM_008958	TCCGCACCTCATATCCTAGC	CTGTCTCAATTACAGCCACTCG
Smo	Smoothened homologue	NM_176996	GCTGGAGTAGTCTGGTTCGT	GAGTCTCCATCTACCTGAGCC
Sostdc1	Sclerostin domain containing 1	NM_025312	CTTCCTCCTGCCATTCATCTC	GAACTCGACTGTTTCGATCCAG
Shh	Sonic hedgehog	NM_009170	GTTTATTCCCAACGTAGCCGA	CTTGTCTTTGCACCTCTGAGTC

phase of the hair cycle. The four hair types were distinguished on the basis of their hair length, number of kinks, and medulla width (Sharov et al., 2006). Hair shaft length and width of ∼250 plucked hair shafts per animal were measured using ImageJ software. Data were pooled, the means ± SD were calculated, and statistical analysis was performed using an unpaired Student's *t* test.

The percentage of HFs in different anagen stages was assessed and calculated in K14-rtTA/TRE-miR-214 at days 3 and 5 after the depilation-induced hair cycle, respectively, as well as in their corresponding WT littermates. All evaluations were performed using accepted, well-defined morphological criteria of HFs at early, mid, and late anagen phase based on the changes in the shape and size of the hair matrix and the dermal papilla (Müller-Röver et al., 2001).

Immunofluorescence intensity was determined using ImageJ software, as described previously (Ramot et al., 2010). In brief, red or green fluorescent signal was collected from experimental tissues in RGB format using the same exposure conditions. To measure the fluorescence intensity at each pixel, the RGB images were converted to 8-bit grayscale format. Regions of interest of distinct size within the WT and DTG HFs were selected, and the mean values of intensity were calculated for each selected areas followed by the normalization relative to the number of DAPI+ cells.

Cell culture and transfections

PMEKs were prepared from newborn mice at P2–3. In brief, mouse skins were incubated in 0.25% trypsin at 4°C overnight. The epidermal portion was minced and filtered through a 70-µm cell strainer (BD Biosciences), which result in a single-cell suspension. PMEKs were grown in EMEM calcium-free medium (Lonza) supplemented with 0.05 mM calcium, at 33°C, 8% CO_2 (Scientific Laboratory Suppliers, Hessle, UK) until 60–70% confluent. PMEKs were transfected with 200 nM of synthetic miR-214 inhibitor (anti-miR-214), miR-214 mimic (pro-miR-214), or miRNA negative controls (GE Healthcare), using Lipofectamine RNAiMax (Invitrogen). Cells were harvested 24 h after transfection and used for further analyses. To induce Wnt signaling, PMEKs were treated with 10 mM lithium chloride (Klein and Melton, 1996). To examine the regulatory effects of miR-214 on Wnt/β-Catenin signaling, PMEKs were treated with 10 mM LiCl for 2 h, followed by transfection of cells with 200 nM pro-miR-214 or miRNA negative controls for 4 h at 33°C, 8% CO_2. Cells were then harvested 24 h after transfection.

miRNA binding predictions

MiR-214 binding was estimated as a consensus from four different prediction algorithms: TargetScan (http://www.targetscan.org/) predicts biological targets of miRNAs by searching for the presence of conserved sites that match the seed region of each miRNA; miRBase (http://microrna.sanger.ac.uk) uses the miRanda algorithm to predict miRNA-mRNA pairs; miRDB (http://mirdb.org/miRDB) uses the MirTarget2 algorithm, which was developed by analyzing thousands of genes impacted by miRNAs; and PITA (http://genie.weizmann.ac.il/pubs/mir07/mir07_data.html) confirms candidates predicted by the other three algorithms.

Luciferase reporter assay

HaCaT cells were grown in Dulbecco's modified Eagle's medium (Invitrogen) supplemented with heat-inactivated 10% FBS in an atmosphere of 5% CO_2 at 37°C, until 60–70% confluent. 3′ UTR fragments of *β-catenin* and *Shh* containing miR-214 putative target sites were amplified from mouse genomic DNA using forward and reverse primers containing XhoI and NotI restriction sequences, respectively. For 3′ UTR of *β-catenin* fragment, 5′-CGAGGAGTAACAATACAAATGG-3′ and 5′-CAGGTTCACTAGAACATAACAC-3′ forward and reverse primers, respectively, were used. To amplify a fragment of the 3′ UTR of *Shh*, 5′-ATGAACGGACCTTCAAGAGC-3′ and 5′-GCATAGCAGGAGAGGAATGC-3′ primers were used. The amplified fragments were cloned at XhoI and NotI sites downstream of CV40 promoter-driven Renilla luciferase cassette in pCHECK2 (Promega). Site-directed mutagenesis was performed using a QuikChange II XL Site-Directed Mutagenesis kit (Agilent Technologies) to mutate the β-catenin binding site according to the manufacturer's instructions. For the dual luciferase assay, these constructs (200 ng) were cotransfected with 200 nM miR-214 mimic or negative control mimic (GE Healthcare) into HaCaT cells using 0.5 µl Lipofectamine 2000 (Invitrogen) in 96-well plates. At 24 h after transfection, the relative luciferase activities were determined using Dual-Glo Luciferase Assay System (Promega). Assay was performed in triplicate for three independent trials.

TOPFlash and FOPFlash Wnt reporter assays

HaCaT cells were seeded onto 12-well dishes 24 h before transfection. At 80% confluence, a TOPFlash Wnt reporter plasmid (plasmid 12456; Addgene) were transfected into each well in combination with (1) control oligonucleotide (200 nM), (2) 10 µM of BIO (R&D Systems), (3) pro–miR-214 (200 nM), and (4) pro–miR-214 (200 nM) and 10 µM BIO (Sato et al., 1999). Transfection was done using Lipofectamine 2000 (Invitrogen). FOPFlash (TOPFlash mutant) reporter plasmid (plasmid 12457; Addgene) was used as a control. The cells were cultured for 24 h. The relative luciferase activities were determined using the Dual-Gloluciferase assay system (Promega) on a microplate reader (Infinite 2000; Tecan). All assays were performed in triplicate for three independent trials.

Online supplemental material

Fig. S1 shows additional details of the skin phenotype in K14-rtTA/miR-214-TRE mice during morphogenesis and the hair cycling, and the results of bioinformatic prediction of miR-214 targets in the keratinocytes and their validation. Tables S1 and S2 list the genes with down- and up-regulated expression in the skin epithelium of K14-rtTA/miR-214-TRE versus WT mice. Online supplemental material is available at http://www.jcb.org/cgi/content/full/jcb.201404001/DC1.

This study was supported by a grant from the Medical Research Council UK (MR/K011324/1) to N.V. Botchkareva.

The authors declare no competing financial interests.

Submitted: 1 April 2014
Accepted: 23 October 2014

References

Ahmed, M.I., A.N. Mardaryev, C.J. Lewis, A.A. Sharov, and N.V. Botchkareva. 2011. MicroRNA-21 is an important downstream component of BMP signalling in epidermal keratinocytes. *J. Cell Sci.* 124:3399–3404. http://dx.doi.org/10.1242/jcs.086710

Ambros, V. 2001. microRNAs: tiny regulators with great potential. *Cell*. 107: 823–826. http://dx.doi.org/10.1016/S0092-8674(01)00616-X

Andl, T., S.T. Reddy, T. Gaddapara, and S.E. Millar. 2002. WNT signals are required for the initiation of hair follicle development. *Dev. Cell*. 2:643–653. http://dx.doi.org/10.1016/S1534-5807(02)00167-3

Andl, T., E.P. Murchison, F. Liu, Y. Zhang, M. Yunta-Gonzalez, J.W. Tobias, C.D. Andl, J.T. Seykora, G.J. Hannon, and S.E. Millar. 2006. The miRNA-processing enzyme dicer is essential for the morphogenesis and maintenance of hair follicles. *Curr. Biol.* 16:1041–1049. http://dx.doi.org/10.1016/j.cub.2006.04.005

Blache, P., M. van de Wetering, I. Duluc, C. Domon, P. Berta, J.N. Freund, H. Clevers, and P. Jay. 2004. SOX9 is an intestine crypt transcription factor, is regulated by the Wnt pathway, and represses the CDX2 and MUC2 genes. *J. Cell Biol.* 166:37–47. http://dx.doi.org/10.1083/jcb.200311021

Blanpain, C., and E. Fuchs. 2009. Epidermal homeostasis: a balancing act of stem cells in the skin. *Nat. Rev. Mol. Cell Biol.* 10:207–217. http://dx.doi.org/10.1038/nrm2636

Botchkarev, V.A., and R. Paus. 2003. Molecular biology of hair morphogenesis: development and cycling. *J. Exp. Zoolog. B Mol. Dev. Evol.* 298B:164–180. http://dx.doi.org/10.1002/jez.b.33

Botchkarev, V.A., N.V. Botchkareva, W. Roth, M. Nakamura, L.H. Chen, W. Herzog, G. Lindner, J.A. McMahon, C. Peters, R. Lauster, et al. 1999. Noggin is a mesenchymally derived stimulator of hair-follicle induction. *Nat. Cell Biol.* 1:158–164. http://dx.doi.org/10.1038/11078

Botchkarev, V.A., M.R. Gdula, A.N. Mardaryev, A.A. Sharov, and M.Y. Fessing. 2012. Epigenetic regulation of gene expression in keratinocytes. *J. Invest. Dermatol.* 132:2505–2521. http://dx.doi.org/10.1038/jid.2012.182

Botchkareva, N.V. 2012. MicroRNA/mRNA regulatory networks in the control of skin development and regeneration. *Cell Cycle*. 11:468–474. http://dx.doi.org/10.4161/cc.11.3.19058

Botchkareva, N.V., V.A. Botchkarev, L.H. Chen, G. Lindner, and R. Paus. 1999. A role for p75 neurotrophin receptor in the control of hair follicle morphogenesis. *Dev. Biol.* 216:135–153. http://dx.doi.org/10.1006/dbio.1999.9464

Byrne, C., M. Tainsky, and E. Fuchs. 1994. Programming gene expression in developing epidermis. *Development*. 120:2369–2383.

Chan, E.F., U. Gat, J.M. McNiff, and E. Fuchs. 1999. A common human skin tumour is caused by activating mutations in β-catenin. *Nat. Genet.* 21:410–413. http://dx.doi.org/10.1038/7747

Chen, H., R. Shalom-Feuerstein, J. Riley, S.D. Zhang, P. Tucci, M. Agostini, D. Aberdam, R.A. Knight, G. Genchi, P. Nicotera, et al. 2010. miR-7 and miR-214 are specifically expressed during neuroblastoma differentiation, cortical development and embryonic stem cells differentiation, and control neurite outgrowth in vitro. *Biochem. Biophys. Res. Commun.* 394:921–927. http://dx.doi.org/10.1016/j.bbrc.2010.03.076

Chi, W., E. Wu, and B.A. Morgan. 2013. Dermal papilla cell number specifies hair size, shape and cycling and its reduction causes follicular decline. *Development*. 140:1676–1683. http://dx.doi.org/10.1242/dev.090662

Chiang, C., R.Z. Swan, M. Grachtchouk, M. Bolinger, Y. Litingtung, E.K. Robertson, M.K. Cooper, W. Gaffield, H. Westphal, P.A. Beachy, and A.A. Dlugosz. 1999. Essential role for Sonic hedgehog during hair follicle morphogenesis. *Dev. Biol.* 205:1–9. http://dx.doi.org/10.1006/dbio.1998.9103

Choi, Y.S., Y. Zhang, M. Xu, Y. Yang, M. Ito, T. Peng, Z. Cui, A. Nagy, A.K. Hadjantonakis, R.A. Lang, et al. 2013. Distinct functions for Wnt/β-catenin in hair follicle stem cell proliferation and survival and interfollicular epidermal homeostasis. *Cell Stem Cell*. 13:720–733. http://dx.doi.org/10.1016/j.stem.2013.10.003

Eivers, E., L.C. Fuentealba, and E.M. De Robertis. 2008. Integrating positional information at the level of Smad1/5/8. *Curr. Opin. Genet. Dev.* 18:304–310. http://dx.doi.org/10.1016/j.gde.2008.06.001

Enshell-Seijffers, D., C. Lindon, M. Kashiwagi, and B.A. Morgan. 2010. β-catenin activity in the dermal papilla regulates morphogenesis and regeneration of hair. *Dev. Cell*. 18:633–642. http://dx.doi.org/10.1016/j.devcel.2010.01.016

Frye, M., and S.A. Benitah. 2012. Chromatin regulators in mammalian epidermis. *Semin. Cell Dev. Biol.* 23:897–905. http://dx.doi.org/10.1016/j.semcdb.2012.08.009

Fu, J., and W. Hsu. 2013. Epidermal Wnt controls hair follicle induction by orchestrating dynamic signaling crosstalk between the epidermis and dermis. *J. Invest. Dermatol.* 133:890–898. http://dx.doi.org/10.1038/jid.2012.407

Garza, L.A., C.C. Yang, T. Zhao, H.B. Blatt, M. Lee, H. He, D.C. Stanton, L. Carrasco, J.H. Spiegel, J.W. Tobias, and G. Cotsarelis. 2011. Bald scalp in men with androgenetic alopecia retains hair follicle stem cells but lacks CD200-rich and CD34-positive hair follicle progenitor cells. *J. Clin. Invest.* 121:613–622. http://dx.doi.org/10.1172/JCI44478

Gunn, W.G., U. Krause, N. Lee, and C.A. Gregory. 2011. Pharmaceutical inhibition of glycogen synthetase kinase-3β reduces multiple myeloma-induced bone disease in a novel murine plasmacytoma xenograft model. *Blood*. 117:1641–1651. http://dx.doi.org/10.1182/blood-2010-09-308171

Hsu, Y.C., and E. Fuchs. 2012. A family business: stem cell progeny join the niche to regulate homeostasis. *Nat. Rev. Mol. Cell Biol.* 13:103–114. http://dx.doi.org/10.1038/nrm3272

Hsu, Y.C., H.A. Pasolli, and E. Fuchs. 2011. Dynamics between stem cells, niche, and progeny in the hair follicle. *Cell*. 144:92–105. http://dx.doi.org/10.1016/j.cell.2010.11.049

Huelsken, J., R. Vogel, B. Erdmann, G. Cotsarelis, and W. Birchmeier. 2001. β-Catenin controls hair follicle morphogenesis and stem cell differentiation in the skin. *Cell*. 105:533–545. http://dx.doi.org/10.1016/S0092-8674(01)00336-1

Inui, M., G. Martello, and S. Piccolo. 2010. MicroRNA control of signal transduction. *Nat. Rev. Mol. Cell Biol.* 11:252–263. http://dx.doi.org/10.1038/nrm2868

Jiang, T.X., Y.H. Liu, R.B. Widelitz, R.K. Kundu, R.E. Maxson, and C.M. Chuong. 1999. Epidermal dysplasia and abnormal hair follicles in transgenic mice overexpressing homeobox gene MSX-2. *J. Invest. Dermatol.* 113:230–237. http://dx.doi.org/10.1046/j.1523-1747.1999.00680.x

Joglekar, M.V., V.S. Parekh, and A.A. Hardikar. 2007. New pancreas from old: microregulators of pancreas regeneration. *Trends Endocrinol. Metab.* 18:393–400. http://dx.doi.org/10.1016/j.tem.2007.10.001

Kertesz, M., N. Iovino, U. Unnerstall, U. Gaul, and E. Segal. 2007. The role of site accessibility in microRNA target recognition. *Nat. Genet.* 39:1278–1284. http://dx.doi.org/10.1038/ng2135

Klein, P.S., and D.A. Melton. 1996. A molecular mechanism for the effect of lithium on development. *Proc. Natl. Acad. Sci. USA*. 93:8455–8459. http://dx.doi.org/10.1073/pnas.93.16.8455

Kwon, Y.J., C.H. Yoon, S.W. Lee, Y.B. Park, S.K. Lee, and M.C. Park. 2014. Inhibition of glycogen synthase kinase-3β suppresses inflammatory responses in rheumatoid arthritis fibroblast-like synoviocytes and collagen-induced arthritis. *Joint Bone Spine*. 81:240–246. http://dx.doi.org/10.1016/j.jbspin.2013.09.006

Lee, R.C., R.L. Feinbaum, and V. Ambros. 1993. The *C. elegans* heterochronic gene lin-4 encodes small RNAs with antisense complementarity to lin-14. *Cell*. 75:843–854. http://dx.doi.org/10.1016/0092-8674(93)90529-Y

Lee, Y.B., I. Bantounas, D.Y. Lee, L. Phylactou, M.A. Caldwell, and J.B. Uney. 2009. Twist-1 regulates the miR-199a/214 cluster during development. *Nucleic Acids Res.* 37:123–128. http://dx.doi.org/10.1093/nar/gkn920

Lena, A.M., R. Shalom-Feuerstein, P. Rivetti di Val Cervo, D. Aberdam, R.A. Knight, G. Melino, and E. Candi. 2008. miR-203 represses 'stemness' by repressing ΔNp63. *Cell Death Differ.* 15:1187–1195. http://dx.doi.org/10.1038/cdd.2008.69

Levy, C., M. Khaled, K.C. Robinson, R.A. Veguilla, P.H. Chen, S. Yokoyama, E. Makino, J. Lu, L. Larue, F. Beermann, et al. 2010. Lineage-specific transcriptional regulation of DICER by MITF in melanocytes. *Cell*. 141:994–1005. http://dx.doi.org/10.1016/j.cell.2010.05.004

Lewis, B.P., C.B. Burge, and D.P. Bartel. 2005. Conserved seed pairing, often flanked by adenosines, indicates that thousands of human genes are microRNA targets. *Cell*. 120:15–20. http://dx.doi.org/10.1016/j.cell.2004.12.035

Lewis, C.J., A.N. Mardaryev, K. Poterlowicz, T.Y. Sharova, A. Aziz, D.T. Sharpe, N.V. Botchkareva, and A.A. Sharov. 2014. Bone morphogenetic protein signaling suppresses wound-induced skin repair by inhibiting keratinocyte proliferation and migration. *J. Invest. Dermatol.* 134:827–837. http://dx.doi.org/10.1038/jid.2013.419

Liu, J., X.J. Luo, A.W. Xiong, Z.D. Zhang, S. Yue, M.S. Zhu, and S.Y. Cheng. 2010. MicroRNA-214 promotes myogenic differentiation by facilitating exit from mitosis via down-regulation of proto-oncogene N-ras. *J. Biol. Chem.* 285:26599–26607. http://dx.doi.org/10.1074/jbc.M110.115824

Liu, J.A., M.H. Wu, C.H. Yan, B.K. Chau, H. So, A. Ng, A. Chan, K.S. Cheah, J. Briscoe, and M. Cheung. 2013. Phosphorylation of Sox9 is required for neural crest delamination and is regulated downstream of BMP and canonical Wnt signaling. *Proc. Natl. Acad. Sci. USA*. 110:2882–2887. http://dx.doi.org/10.1073/pnas.1211747110

Malanchi, I., H. Peinado, D. Kassen, T. Hussenet, D. Metzger, P. Chambon, M. Huber, D. Hohl, A. Cano, W. Birchmeier, and J. Huelsken. 2008. Cutaneous cancer stem cell maintenance is dependent on β-catenin signalling. *Nature*. 452:650–653. http://dx.doi.org/10.1038/nature06835

Mardaryev, A.N., M.I. Ahmed, N.V. Vlahov, M.Y. Fessing, J.H. Gill, A.A. Sharov, and N.V. Botchkareva. 2010. Micro-RNA-31 controls hair cycle-associated changes in gene expression programs of the skin and hair follicle. *FASEB J.* 24:3869–3881. http://dx.doi.org/10.1096/fj.10-160663

Meijer, L., A.L. Skaltsounis, P. Magiatis, P. Polychronopoulos, M. Knockaert, M. Leost, X.P. Ryan, C.A. Vonica, A. Brivanlou, R. Dajani, et al. 2003. GSK-3-selective inhibitors derived from Tyrian purple indirubins. *Chem. Biol.* 10:1255–1266. http://dx.doi.org/10.1016/j.chembiol.2003.11.010

Mill, P., R. Mo, H. Fu, M. Grachtchouk, P.C. Kim, A.A. Dlugosz, and C.C. Hui. 2003. Sonic hedgehog-dependent activation of Gli2 is essential for embryonic hair follicle development. *Genes Dev.* 17:282–294. http://dx.doi.org/10.1101/gad.1038103

Millar, S.E. 2002. Molecular mechanisms regulating hair follicle development. *J. Invest. Dermatol.* 118:216–225. http://dx.doi.org/10.1046/j.0022-202x.2001.01670.x

Mou, C., B. Jackson, P. Schneider, P.A. Overbeek, and D.J. Headon. 2006. Generation of the primary hair follicle pattern. *Proc. Natl. Acad. Sci. USA*. 103:9075–9080. http://dx.doi.org/10.1073/pnas.0600825103

Müller-Röver, S., B. Handjiski, C. van der Veen, S. Eichmüller, K. Foitzik, I.A. McKay, K.S. Stenn, and R. Paus. 2001. A comprehensive guide for the accurate classification of murine hair follicles in distinct hair cycle stages. *J. Invest. Dermatol.* 117:3–15. http://dx.doi.org/10.1046/j.0022-202x.2001.01377.x

Ning, M.S., and T. Andl. 2013. Control by a hair's breadth: the role of microRNAs in the skin. *Cell. Mol. Life Sci.* 70:1149–1169. http://dx.doi.org/10.1007/s00018-012-1117-z

Paus, R., S. Müller-Röver, C. Van Der Veen, M. Maurer, S. Eichmüller, G. Ling, U. Hofmann, K. Foitzik, L. Mecklenburg, and B. Handjiski. 1999. A comprehensive guide for the recognition and classification of distinct stages of hair follicle morphogenesis. *J. Invest. Dermatol.* 113:523–532. http://dx.doi.org/10.1046/j.1523-1747.1999.00740.x

Plouhinec, J.L., L. Zakin, and E.M. De Robertis. 2011. Systems control of BMP morphogen flow in vertebrate embryos. *Curr. Opin. Genet. Dev.* 21:696–703. http://dx.doi.org/10.1016/j.gde.2011.09.001

Pummila, M., I. Fliniaux, R. Jaatinen, M.J. James, J. Laurikkala, P. Schneider, I. Thesleff, and M.L. Mikkola. 2007. Ectodysplasin has a dual role in ectodermal organogenesis: inhibition of Bmp activity and induction of Shh expression. *Development*. 134:117–125. http://dx.doi.org/10.1242/dev.02708

Ramot, Y., T. Bíró, S. Tiede, B.I. Tóth, E.A. Langan, K. Sugawara, K. Foitzik, A. Ingber, V. Goffin, L. Langbein, and R. Paus. 2010. Prolactin—a novel neuroendocrine regulator of human keratin expression in situ. *FASEB J.* 24:1768–1779. http://dx.doi.org/10.1096/fj.09-146415

Rehmsmeier, M., P. Steffen, M. Hochsmann, and R. Giegerich. 2004. Fast and effective prediction of microRNA/target duplexes. *RNA*. 10:1507–1517. http://dx.doi.org/10.1261/rna.5248604

Rompolas, P., and V. Greco. 2014. Stem cell dynamics in the hair follicle niche. *Semin. Cell Dev. Biol.* 25-26:34–42. http://dx.doi.org/10.1016/j.semcdb.2013.12.005

Sato, N., P.L. Leopold, and R.G. Crystal. 1999. Induction of the hair growth phase in postnatal mice by localized transient expression of Sonic hedgehog. *J. Clin. Invest.* 104:855–864. http://dx.doi.org/10.1172/JCI7691

Sato, N., L. Meijer, L. Skaltsounis, P. Greengard, and A.H. Brivanlou. 2004. Maintenance of pluripotency in human and mouse embryonic stem cells through activation of Wnt signaling by a pharmacological GSK-3-specific inhibitor. *Nat. Med.* 10:55–63. http://dx.doi.org/10.1038/nm979

Schmidt-Ullrich, R., and R. Paus. 2005. Molecular principles of hair follicle induction and morphogenesis. *BioEssays*. 27:247–261. http://dx.doi.org/10.1002/bies.20184

Schmidt-Ullrich, R., D.J. Tobin, D. Lenhard, P. Schneider, R. Paus, and C. Scheidereit. 2006. NF-κB transmits Eda A1/EdaR signalling to activate Shh and cyclin D1 expression, and controls post-initiation hair placode down growth. *Development*. 133:1045–1057. http://dx.doi.org/10.1242/dev.02278

Schneider, M.R., R. Schmidt-Ullrich, and R. Paus. 2009. The hair follicle as a dynamic miniorgan. *Curr. Biol.* 19:R132–R142. http://dx.doi.org/10.1016/j.cub.2008.12.005

Sehic, A., S. Risnes, C. Khuu, Q.E. Khan, and H. Osmundsen. 2011. Effects of in vivo transfection with anti-miR-214 on gene expression in murine molar tooth germ. *Physiol. Genomics*. 43:488–498. http://dx.doi.org/10.1152/physiolgenomics.00248.2010

Sharov, A.A., T.Y. Sharova, A.N. Mardaryev, A. Tommasi di Vignano, R. Atoyan, L. Weiner, S. Yang, J.L. Brissette, G.P. Dotto, and V.A. Botchkarev. 2006. Bone morphogenetic protein signaling regulates the size of hair follicles and modulates the expression of cell cycle-associated genes. *Proc. Natl. Acad. Sci. USA*. 103:18166–18171. http://dx.doi.org/10.1073/pnas.0608899103

Sick, S., S. Reinker, J. Timmer, and T. Schlake. 2006. WNT and DKK determine hair follicle spacing through a reaction-diffusion mechanism. *Science*. 314:1447–1450. http://dx.doi.org/10.1126/science.1130088

Smyth, G. 2005. Limma: linear models for microarray data. *In* Bioinformatics and Computational Biology Solutions using R and Bioconductor. V.C.R. Gentleman, S. Dudoit, R. Irizarry, and W. Huber, editors. Springer, New York. 397–420. http://dx.doi.org/10.1007/0-387-29362-0_23

St-Jacques, B., H.R. Dassule, I. Karavanova, V.A. Botchkarev, J. Li, P.S. Danielian, J.A. McMahon, P.M. Lewis, R. Paus, and A.P. McMahon. 1998. Sonic hedgehog signaling is essential for hair development. *Curr. Biol.* 8:1058–1069. http://dx.doi.org/10.1016/S0960-9822(98)70443-9

Stenn, K.S., and R. Paus. 2001. Controls of hair follicle cycling. *Physiol. Rev.* 81:449–494.

Su, X., D. Chakravarti, M.S. Cho, L. Liu, Y.J. Gi, Y.L. Lin, M.L. Leung, A. El-Naggar, C.J. Creighton, M.B. Suraokar, et al. 2010. TAp63 suppresses metastasis through coordinate regulation of Dicer and miRNAs. *Nature*. 467:986–990. http://dx.doi.org/10.1038/nature09459

Teta, M., Y.S. Choi, T. Okegbe, G. Wong, O.H. Tam, M.M. Chong, J.T. Seykora, A. Nagy, D.R. Littman, T. Andl, and S.E. Millar. 2012. Inducible deletion of epidermal Dicer and Drosha reveals multiple functions for miRNAs in postnatal skin. *Development*. 139:1405–1416. http://dx.doi.org/10.1242/dev.070920

Tsai, S.Y., R. Sennett, A. Rezza, C. Clavel, L. Grisanti, R. Zemla, S. Najam, and M. Rendl. 2014. Wnt/β-catenin signaling in dermal condensates is required for hair follicle formation. *Dev. Biol.* 385:179–188. http://dx.doi.org/10.1016/j.ydbio.2013.11.023

Vidal, V.P., M.C. Chaboissier, S. Lützkendorf, G. Cotsarelis, P. Mill, C.C. Hui, N. Ortonne, J.P. Ortonne, and A. Schedl. 2005. Sox9 is essential for outer root sheath differentiation and the formation of the hair stem cell compartment. *Curr. Biol.* 15:1340–1351. http://dx.doi.org/10.1016/j.cub.2005.06.064

Wang, X., and I.M. El Naqa. 2008. Prediction of both conserved and nonconserved microRNA targets in animals. *Bioinformatics*. 24:325–332. http://dx.doi.org/10.1093/bioinformatics/btm595

Wang, B., J.F. Fallon, and P.A. Beachy. 2000. Hedgehog-regulated processing of Gli3 produces an anterior/posterior repressor gradient in the developing vertebrate limb. *Cell*. 100:423–434. http://dx.doi.org/10.1016/S0092-8674(00)80678-9

Wang, X., J. Chen, F. Li, Y. Lin, X. Zhang, Z. Lv, and J. Jiang. 2012. MiR-214 inhibits cell growth in hepatocellular carcinoma through suppression of β-catenin. *Biochem. Biophys. Res. Commun.* 428:525–531. http://dx.doi.org/10.1016/j.bbrc.2012.10.039

Wang, D., Z. Zhang, E. O'Loughlin, L. Wang, X. Fan, E.C. Lai, and R. Yi. 2013a. MicroRNA-205 controls neonatal expansion of skin stem cells by modulating the PI(3)K pathway. *Nat. Cell Biol.* 15:1153–1163. http://dx.doi.org/10.1038/ncb2827

Wang, X., B. Guo, Q. Li, J. Peng, Z. Yang, A. Wang, D. Li, Z. Hou, K. Lv, G. Kan, et al. 2013b. miR-214 targets ATF4 to inhibit bone formation. *Nat. Med.* 19:93–100. http://dx.doi.org/10.1038/nm.3026

Watanabe, T., T. Sato, T. Amano, Y. Kawamura, N. Kawamura, H. Kawaguchi, N. Yamashita, H. Kurihara, and T. Nakaoka. 2008. Dnm3os, a non-coding RNA, is required for normal growth and skeletal development in mice. *Dev. Dyn.* 237:3738–3748. http://dx.doi.org/10.1002/dvdy.21787

Yamane, K., M. Jinnin, T. Etoh, Y. Kobayashi, N. Shimozono, S. Fukushima, S. Masuguchi, K. Maruo, Y. Inoue, T. Ishihara, et al. 2013. Down-regulation of miR-124/-214 in cutaneous squamous cell carcinoma mediates abnormal cell proliferation via the induction of ERK. *J. Mol. Med.* 91:69–81. http://dx.doi.org/10.1007/s00109-012-0935-7

Yi, R., and E. Fuchs. 2011. MicroRNAs and their roles in mammalian stem cells. *J. Cell Sci.* 124:1775–1783. http://dx.doi.org/10.1242/jcs.069104

Yi, R., D. O'Carroll, H.A. Pasolli, Z. Zhang, F.S. Dietrich, A. Tarakhovsky, and E. Fuchs. 2006. Morphogenesis in skin is governed by discrete sets of differentially expressed microRNAs. *Nat. Genet.* 38:356–362. http://dx.doi.org/10.1038/ng1744

Yi, R., M.N. Poy, M. Stoffel, and E. Fuchs. 2008. A skin microRNA promotes differentiation by repressing 'stemness'. *Nature*. 452:225–229. http://dx.doi.org/10.1038/nature06642

Zhang, Y., P. Tomann, T. Andl, N.M. Gallant, J. Huelsken, B. Jerchow, W. Birchmeier, R. Paus, S. Piccolo, M.L. Mikkola, et al. 2009. Reciprocal requirements for EDA/EDAR/NF-kappaB and Wnt/β-catenin signaling pathways in hair follicle induction. *Dev. Cell*. 17:49–61. http://dx.doi.org/10.1016/j.devcel.2009.05.011

Zhang, L., N. Stokes, L. Polak, and E. Fuchs. 2011. Specific microRNAs are preferentially expressed by skin stem cells to balance self-renewal and early lineage commitment. *Cell Stem Cell*. 8:294–308. http://dx.doi.org/10.1016/j.stem.2011.01.014

Zhou, P., C. Byrne, J. Jacobs, and E. Fuchs. 1995. Lymphoid enhancer factor 1 directs hair follicle patterning and epithelial cell fate. *Genes Dev.* 9:700–713. http://dx.doi.org/10.1101/gad.9.6.700

Zhou, J.X., L.W. Jia, W.M. Liu, C.L. Miao, S. Liu, Y.J. Cao, and E.K. Duan. 2006. Role of sonic hedgehog in maintaining a pool of proliferating stem cells in the human fetal epidermis. *Hum. Reprod.* 21:1698–1704. http://dx.doi.org/10.1093/humrep/del086

Zhu, H., and G.C. Fan. 2011. Extracellular/circulating microRNAs and their potential role in cardiovascular disease. *Am. J. Cardiovasc. Dis*. 1:138–149.